CONFIDENTIAL

Copy 321
RM H55E16

NACA RM H55E16

NACA

RESEARCH MEMORANDUM

STABILITY AND CONTROL CHARACTERISTICS OBTAINED DURING DEMONSTRATION OF THE DOUGLAS X-3 RESEARCH AIRPLANE

By Richard E. Day and Jack Fischel

High-Speed Flight Station
Edwards, Calif.

CLASSIFIED DOCUMENT

NATIONAL ADVISORY COMMITTEE
FOR AERONAUTICS

WASHINGTON

July 21, 1955

CONFIDENTIAL

NATIONAL ADVISORY COMMITTEE FOR AERONAUTICS

RESEARCH MEMORANDUM

STABILITY AND CONTROL CHARACTERISTICS OBTAINED DURING DEMONSTRATION OF THE DOUGLAS X-3 RESEARCH AIRPLANE

By Richard E. Day and Jack Fischel

SUMMARY

Flight tests were performed with the Douglas X-3 research airplane during the manufacturer's demonstration program and for U. S. Air Force evaluation. These tests covered the Mach number range to 1.21 and an altitude range from 12,800 feet to 34,000 feet. Longitudinal, lateral, and directional stability and control data obtained during these tests in steady flight and maneuvering flight are presented in this paper and are compared with wind-tunnel and rocket-model data.

Longitudinal control deflection required to trim the airplane over the Mach number range was generally similar to that of other airplanes, characterized by a stable variation at Mach numbers below 0.92 and a slight nose-down trim change at Mach numbers above 1.07.

Data obtained during turns and pull-ups indicated that throughout the Mach number range from 0.65 to 1.21, the apparent static longitudinal stability was positive at low lifts and increased by a factor of about $2\frac{1}{2}$ as Mach number was increased from 0.9 to 1.2. The apparent stability exhibited a gradual decrease as lift increased and mild pitch-ups occurred at Mach numbers above 0.95. The pitch-ups occurred at normal-force coefficients of about 0.7 to 0.8, which is slightly below maximum wing lift at a Mach number of approximately 0.95, and about 0.4 to 0.3 below maximum wing lift at Mach numbers greater than 1.0.

Difficulty was experienced in performing smooth longitudinal maneuvers. This condition appeared to result from the combination of control system, pilot, airplane, and their dynamic characteristics; however, additional tests are required to determine the primary cause of the lag and oscillations experienced.

Unaccelerated stalls appeared stable in all configurations tested, except at large angles of attack in the landing configuration where some

instability was evident. Roll-off tendencies, which became more severe as the speed was decreased, were apparent in all configurations.

Data obtained during sideslips at Mach numbers from 0.84 to 0.98 showed the apparent directional stability to be positive and to increase with increase in Mach number. A smaller degree of apparent stability existed for small angles of sideslip than existed for larger angles.

Meager aileron effectiveness data obtained at Mach numbers of 0.89 to 0.98 indicated that the control effectiveness was generally linear with deflection and exhibited little change with increase in Mach number.

Comparison of flight data with wind-tunnel and rocket-model tests showed similar trends and good quantitative agreement.

INTRODUCTION

The Douglas X-3 airplane is one of the series of research airplanes obtained by the U. S. Air Force for the joint Air Force—Navy—National Advisory Committee for Aeronautics high-speed flight research program. The X-3 airplane was designed to investigate the characteristics at supersonic speeds of an airplane having a thin, straight, low-aspect-ratio wing with hexagonal sections. The airplane is single place and is powered by two turbojet engines with afterburners. With the engines presently installed the airplane is limited to near-sonic speeds in level flight although supersonic speeds can be attained by diving.

The purpose of this paper is to present the stability and control characteristics of the X-3 airplane measured during the manufacturer's program to demonstrate the structural integrity of the airplane and the proper functioning of the various airplane systems. Data from two U. S. Air Force evaluation flights are also included. All the data presented in this paper were obtained from NACA research instrumentation which was employed during the entire program. The data cover the Mach number range to 1.21 and were obtained during trimmed-flight speed runs; longitudinal, directional, and lateral maneuvers; and unaccelerated stalls. Comparison of the flight data with data obtained during wind-tunnel and free-flight investigations of X-3 models is included. Lift and drag data obtained concurrently on the X-3 airplane during the demonstration and evaluation flights are reported in reference 1.

SYMBOLS

a_t	transverse acceleration, g units
b	wing span, ft
C_L	lift coefficient, $L/\frac{1}{2}\rho V^2 S$
C_{L_α}	slope of lift curve per degree, $dC_L/d\alpha$
C_{N_A}	airplane normal-force coefficient, $nW/\frac{1}{2}\rho V^2 S$
$C_{N_{A_\alpha}}$	slope of airplane normal-force-coefficient curve per degree, $dC_{N_A}/d\alpha$
C_Y	lateral-force coefficient, $a_t W/\frac{1}{2}\rho V^2 S$
C_{Y_β}	slope of lateral-force-coefficient curve per degree of sideslip angle, $dC_Y/d\beta$
C_m	pitching-moment coefficient
c	wing chord, in.
$\bar{c}$	mean aerodynamic chord, in.
F_a	aileron control wheel force, lb
F_r	rudder pedal force, lb
F_s	stabilizer control column force, lb
g	acceleration due to gravity, ft/sec^2
h_p	pressure altitude, ft
i_t	stabilizer deflection with respect to fuselage reference line, leading edge of stabilizer up is positive, deg
L	lift, lb

M	free-stream Mach number
n	normal load factor or acceleration, g units
P	free-stream static pressure, lb/sq ft
p	rolling angular velocity, radians/sec
q	pitching angular velocity, radians/sec
r	yawing angular velocity, radians/sec
S	wing area, sq ft
V	true airspeed, ft/sec
V_i	indicated airspeed, knots
W	airplane weight, lb
α	angle of attack, deg
β	angle of sideslip, deg
δ_a	total aileron deflection, right roll positive, deg
$\delta_{f_{le}}$	leading-edge flap deflection, deg
$\delta_{f_{te}}$	trailing-edge flap deflection, deg
δ_r	rudder deflection, deg
δ_{p_L}	left rudder pedal deflection, in.
δ_{w_a}	aileron control wheel rotation, deg
δ_{w_s}	stabilizer control column travel, in.
ρ	mass density of air, slugs/cu ft
$1/2\rho V^2$	free-stream dynamic pressure, lb/sq ft
di_t/dC_L	apparent longitudinal stability parameter, deg

di_t/dC_{N_A} apparent longitudinal stability parameter, deg

$d\delta_a/d\beta$ apparent effective dihedral parameter

$d\delta_r/d\beta$ apparent directional stability parameter

$pb/2V$ wing-tip helix angle, radians

DESCRIPTION OF AIRPLANE

The Douglas X-3 research airplane is a single-place straight-wing airplane powered by two J34 turbojet engines equipped with afterburners. The airplane is also characterized by a long fuselage with an appreciable frontal area to wing area ratio. Photographs of the airplane are shown in figure 1 and figure 2. A three-view drawing is presented in figure 3. Additional airplane dimensions are given in table I. The low midwing has an aspect ratio of 3.1, is unswept at the 75-percent-chord line, and is equipped with both leading- and trailing-edge flaps. The airfoil employed for the wing is a $4\frac{1}{2}$-percent-thick modified hexagonal section normal to the 75-percent-chord station (fig. 3).

The airplane has an all-movable horizontal tail surface and conventional flap-type rudder and aileron control surfaces. All the aerodynamic control surfaces are powered by an irreversible hydraulic system and have variable artificial force gradients. The horizontal tail has fixed tabs to alleviate hinge moments for the condition of hydraulic system failure. Preloaded springs are used in the control system to provide a variation of control force with control deflection. A dynamic-static pressure sensing unit changes the mechanical advantage between the cockpit controls and the feel springs, producing control-force gradients as shown in figure 4.

Provision is also included for varying stabilizer control-force gradients provided by the preloaded springs independent of the dynamic-static pressure sensing unit. The control-force friction appears to increase somewhat with increase in the control-force gradient (F_s/i_t).

INSTRUMENTATION

The following pertinent quantities were recorded on NACA internal recording instruments which were synchronized by a common timer:

Airspeed and altitude

Normal and transverse acceleration

Rolling angular velocity

Pitching angular velocity

Yawing angular velocity

Angle of attack and angle of sideslip

Control column, control wheel, and rudder pedal positions

Stabilizer, aileron, and rudder positions

Stabilizer, aileron, and rudder control forces

Leading- and trailing-edge flap positions

The angle of attack and stabilizer deflection were measured relative to the fuselage horizontal reference plane. The vanes used to measure the angle of attack and the angle of sideslip were mounted on a boom approximately $2\frac{3}{4}$ feet and $2\frac{1}{4}$ feet, respectively, forward of the nose of the airplane (fig. 5). The values presented for angle of attack were not corrected for the effects of upwash ahead of the nose of the airplane nor for the effects of boom bending or pitching velocity. The pitching velocities encountered were not sufficiently high to change appreciably the recorded values.

A Douglas airspeed head was mounted on the boom about $4\frac{1}{2}$ feet forward of the nose of the airplane (fig. 5). The differential pressure probes on the nose of the boom were part of the instrumentation of the Douglas Aircraft Co. and were not used for the data of this paper. The airspeed system was calibrated by using the NACA radar-phototheodolite method of reference 2. The accuracy of the Mach numbers obtained is believed to be within ± 0.01.

TESTS

The data presented in this paper were obtained during demonstration flights by the Douglas Aircraft Co. and during preliminary U. S. Air Force evaluation flights. Consequently, the lift and Mach number ranges

covered in obtaining various stability and control parameters are not complete, particularly for the directional and lateral stability survey.

Longitudinal trim data ranging from $M = 0.60$ to $M = 1.16$ were obtained from stall approaches, level-flight speed runs, and dives with the airplane in the clean configuration. Static longitudinal stability and control characteristics in accelerated flight were determined with the airplane in the clean configuration during wind-up turns at Mach numbers from 0.63 to 0.94, and during pull-outs at Mach numbers from 0.94 to 1.21. Stall approaches were performed with various combinations of leading- and trailing-edge flap deflections with gear up or gear down. Static directional and lateral stability data were obtained from right and left gradually increasing wing-level sideslips at Mach numbers of 0.84, 0.96, and 0.98. Lateral control effectiveness characteristics were obtained between $M = 0.89$ and $M = 0.98$ from rudder-fixed aileron rolls at various aileron deflections.

The data were obtained at pressure altitudes ranging from 12,800 feet to 34,000 feet. The center-of-gravity positions for these tests were within the limits of 3 percent and -2 percent of the mean aerodynamic chord. A more precise determination of the center-of-gravity position was limited by the existing instrumentation (pertinent to fuel consumption).

RESULTS AND DISCUSSION

Trim Characteristics

Figure 6 shows the longitudinal control-surface deflections required to trim the airplane in 1 g flight through the usable Mach number range. These data were obtained during level runs, dives, and stalls. The values of stabilizer deflection were corrected to constant conditions of 1 g flight at a pressure altitude of 30,000 feet and a wing loading of 116 pounds per square foot by using the values of the parameter di_t/dC_{N_A} obtained during turns and pull-ups. The variation of trim-stabilizer deflection with Mach number (fig. 6) indicates that the airplane exhibits a longitudinally stable trend from Mach numbers of 0.6 to about 0.92, followed by a neutrally stable region to $M = 0.97$. A nose-up trim change occurs starting at a Mach number of approximately 0.97 with the highest rate of change of trim deflection near a Mach number of 1.0. A slight nose-down trim change then occurs from Mach numbers of about 1.07 to 1.16, the highest Mach number at which trim data were obtained. The longitudinal control forces for trimming the airplane are not presented because various trim settings were used during the several flights traversing the Mach number range shown.

Adequate data are not available to present the lateral trim requirements over the Mach number range; however, the pilots reported the occurrence of slight inconsistent trim changes at a Mach number of about 0.95.

Longitudinal Stability and Control Characteristics in Accelerated Maneuvers

Data obtained during several accelerated maneuvers, representing the lift and Mach number ranges covered, are presented as time histories in figure 7. Figure 8 presents these data in the form of stability cross plots. Additional data obtained during other accelerated longitudinal maneuvers are not presented in this paper but were used to determine the values of various stability parameters over the Mach number range. In general, because of the buffeting and the proximity of wing maximum lift (as shown by wing loads measurements in subsequent maneuvers), the maneuvers performed at Mach numbers less than 0.9 were over a lift range extending only to C_{N_A} of about 0.5 to 0.6. At Mach numbers greater than 0.9 the maneuvers were generally over a larger lift range extending as high as $C_{N_A} = 1.1$.

The longitudinal oscillations evident in figure 7 are caused by a combination of characteristics of the control system, pilot, and airplane. Sufficient dynamic characteristics have not been obtained to evaluate these oscillations in detail and, although the airplane longitudinal damping appears high, it is felt that more tests are needed to determine the primary contributor to the sustained oscillations experienced. Some contributing factors of the oscillations may be indicated. An inspection of the time-history plots (particularly figs. 7(b) and 7(d)) indicates that the summation of incremental time lags between application of stabilizer wheel force, movement of the stabilizer control wheel, change in tail incidence, and change in airplane angle of attack is as much as 1 second, causing the application of control force to be as much as 180° out of phase with the airplane response. Examination of time histories (fig. 7) and plots of stabilizer deflection as a function of stabilizer control-wheel position (fig. 8) indicates by their linearity that loss of motion in the control hydraulic system (such as caused by inertia of hydraulic system and control components) or control cable stretch (between the stabilizer control wheel and the stabilizer-actuating-hydraulic cylinder) is a minor contribution to the phase lag (approximately 0.1 to 0.2 sec.). Additional effects shown in figure 7 are the appreciable control force changes occurring during the low-speed maneuvers with little or no corresponding changes in cockpit control position or stabilizer deflection and the continuance of stabilizer motion during several of the maneuvers when the force was stopped or reversed. These effects result from the control-feel system friction

and breakout forces which are larger for the maximum spring load-feel gradients employed for these maneuvers (except for fig. 7(c), discussed subsequently), and also from hydraulic valve friction in the powered control system (ref. 3). These effects are believed to contribute appreciably to the lag and oscillatory characteristics shown. A large phase difference is also apparent between the deflection of the stabilizer and change in airplane attitude as represented by angle of attack (fig. 7); however, the actual lag in development of pitching velocity, about 0.2 second, is normal.

Because of the oscillations encountered during the longitudinal maneuvers, analysis of the airplane stability is difficult particularly at Mach numbers less than 0.9 where the range of C_{N_A} covered was very limited. However, examination of the plots of stabilizer deflection against angle of attack and C_{N_A} at the higher Mach numbers (figs. 8(c) and 8(e)) shows the apparent stick-fixed stability to be positive, as indicated by the negative slope of the curves of i_t plotted against α, but nonlinear over most of the angle-of-attack range. The apparent stability decreased and approached neutral stability at the higher values of α and C_{N_A}. At Mach numbers above about 0.95, pitch-up was experienced with the airplane during the longitudinal maneuvers. The data of figures 7(d) to 7(f) and 8(d) to 8(f) show that the pitch-up was probably aggravated by the lag and oscillations previously discussed. Figure 7(f), for example, illustrates a pitch-up beginning at time 4.0 seconds. As the stabilizer column position and stabilizer deflection became nearly constant, an overshoot in angle of attack of about 8° and in acceleration of about 3 g occurred, accompanied by a relatively low pitching velocity of approximately 0.2 radian per second. (Also see fig. 8(f).) Although the pitching velocities and accelerations experienced in the pitch-ups were considered by the pilots to be reasonably mild, large values of pitching acceleration were sometimes attained during the subsequent recovery when excessive control rates were used. In general, pitch-up was apparent at normal-force coefficients of about 0.7 to 0.8 at all Mach numbers above 0.95. These values of normal-force coefficient were slightly below maximum wing lift (as obtained from wing-loads measurements) at $M \approx 0.95$ and about 0.4 to 0.3 below maximum wing lift at Mach numbers greater than 1.0.

To illustrate the changes in stability occurring over the angle-of-attack range in terms of airplane pitching-moment coefficient, the flight data of figures 7(f) and 8(f) have been reduced to values of C_m by an analysis similar to that employed in reference 4 and are presented in figure 9. As discussed in the preceding paragraph, the plots of figure 9 show the stability is initially positive at low values of α and C_{N_A} but tends to decrease and become negative as α is increased, resulting

in the pitch-up experienced in flight. Some of the indicated changes in stability over the angle-of-attack range may result from the changes in Mach number occurring during the course of the maneuver (fig. 7(f)). In addition, a comparison was made of the static margin at low lifts for the flight data of figure 9 and the wind-tunnel data of reference 5 (interpolated for $M \approx 1.17$). This comparison showed good agreement.

For most of the maneuvers evaluated, the pressure-sensing control-force unit was not used and the stabilizer load feel was manually set to maximum. Consequently, the apparent stick-free stability is essentially the same as the stick-fixed stability pattern inasmuch as the synthetic feel system, consisting essentially of a spring arrangement, produces a linear control force—surface deflection gradient. The stabilizer wheel force, shown as a function of normal load factor in figure 8, gives an approximate value of 20 pounds per unit acceleration for the maximum load-feel conditions stated previously (figs. 8(d) to 8(f)). Data from one of the three turns in which automatic load feel was used are shown in figure 8(c). The control-force gradient under these conditions and at the specified altitude has been reduced to approximately 8 pounds per unit acceleration.

The apparent stability parameter di_t/dC_{N_A} is shown in figure 10 as a function of Mach number at a constant C_{N_A} of 0.3. For comparison the solid line in figure 10 gives wind-tunnel values, taken from reference 5, for di_t/dC_L as a function of Mach number at a constant value of $C_L = 0.3$ and $i_t = 0^\circ$. Both sets of data were obtained at about the same center-of-gravity position, approximately $0\bar{c}$. At Mach numbers less than 0.9 insufficient flight data are available to define adequately the variation of the apparent stability parameter with Mach number. However, values of approximately -5° were obtained below $M = 0.9$. The negative value then appears to increase linearly with Mach number from a value of about -6° at $M = 0.93$ to a value of -12° at $M = 1.21$, indicating either an increase in airplane stability or a decrease in stabilizer effectiveness, or both. Although figure 10 shows wind-tunnel data are not available in the range of Mach number where most of the flight data were obtained, the agreement shown in trend and level of the values of di_t/dC_{N_A} and di_t/dC_L appears fairly good.

The variation with Mach number of the airplane normal-force-coefficient-curve slope $C_{N_{A_\alpha}}$ obtained at a value of $C_{N_A} \approx 0.3$ during accelerated maneuvers (figs. 7 and 8) is shown in figure 11. Also presented in figure 11 is the variation of C_{L_α} with Mach number obtained during wind-tunnel model tests (ref. 5) and rocket-model tests (ref. 6) at $C_L \approx 0.3$. The flight values of $C_{N_{A_\alpha}}$ increase from about 0.075 at

$M = 0.65$ to about 0.105 at $M = 1.0$, then decrease to about 0.095 at $M = 1.2$. Although the flight data agree in trend with the rocket- and wind-tunnel data presented, flight values of $C_{N_{A_\alpha}}$ are higher over the entire Mach number range shown. One possible reason for the higher flight values of $C_{N_{A_\alpha}}$ is the fact that flight values of α were not corrected for boom bending, pitching velocity, or other conditions.

Stalling Characteristics

Data obtained during unaccelerated stall approaches (made at $h_p \approx 26{,}000$ ft) for three airplane configurations are presented in figure 12 in the form of time histories of the measured quantities. In figure 13 several quantities are presented as a function of indicated airspeed. Figure 14 shows i_t and C_{N_A} as functions of angle of attack. In all flap and gear configurations the airplane flew unsteadily both laterally and longitudinally during the stalls (fig. 12). This behavior appeared to be control induced to a large extent; however, rapid oscillations of the ailerons can be observed during the early part of the stall shown on figure 12(c) with little or no resulting airplane rolling response. The pilots reported the airplane exhibited poor aileron-control response at low speeds, however, the low-speed aileron-control characteristics have not yet been evaluated. In general, the rolling motions of the airplane were the most severe, especially near the stall where a roll-off tendency was apparent. In the clean condition (flaps and landing gear retracted), the stall approach was started at an indicated airspeed of 361 knots with the stall occurring at about 222 knots (figs. 12(a) and 13(a)). Deflecting the leading-edge flaps to 30° and the trailing-edge flaps to 50° and extending the landing gear resulted in a decrease in stalling speed to about 160 knots (figs. 12(b) and 13(b)). However, deflecting only the leading-edge flaps to 7° (gear retracted) decreased stalling speed to about 206 knots (figs. 12(c) and 13(c)).

The scatter of data points in figure 14, for the curves of stabilizer deflection plotted against angle of attack, is due largely to the erratic control motions and to the inertia lag described previously. Nevertheless, it is evident that the apparent stability gradient $di_t/d\alpha$ is positive in all configurations tested except for some instability exhibited at values of angle of attack greater than 14° in the landing configuration. It is also evident that a higher degree of stability exists for the clean configuration than exists for the landing configuration or for moderate nose flap deflections. (Compare also the variations of i_t with V_i for each configuration in fig. 13.) The wind-tunnel

data of reference 7 indicate the same general effects of deflecting leading- and trailing-edge flaps on the airplane stability.

The curves of airplane normal-force coefficient presented as a function of angle of attack in figure 14 show the variation of C_{N_A} with α to be fairly linear up to the wing stall angle for each configuration. In the clean condition the wing stall occurred at about $C_{N_A} = 0.6$ and $\alpha = 12^\circ$. With leading-edge flaps deflected 7° the stall was delayed to $C_{N_A} \approx 0.7$ and $\alpha \approx 14^\circ$. During the stall approach in the landing configuration, values of $C_{N_A} = 1.19$ and $\alpha = 18.4^\circ$ were attained. These values still appear to be in the linear range of the $C_{N_{A_\alpha}}$ curve.

In general, the values of C_{N_A} and α at which the break or leveling-off occurred in the airplane normal-force-coefficient curve for each configuration were in close agreement with the results of the wind-tunnel investigation of reference 7. In this investigation (ref. 7) an X-3 airplane model with a horizontal tail of aspect ratio 4.0 was employed.

Stick-free characteristics of the airplane during the stall approaches are difficult to evaluate because of the aforementioned oscillations and erratic control motions and also because of the relatively large breakout forces and the friction band of the control system. However, the average forces are quite low during each maneuver and the general trend of the control-force envelope shows a slightly stable to neutral slope in figures 12 and 13 indicating near-neutral stick-free stability for the stall approaches. An exception to this condition may be noted for the landing configuration (figs. 12(b) and 13(b)) where the control forces appear unstable above $\alpha \approx 14^\circ$. In addition, the pilots commented that severe buffeting occurred prior to the stall usually at or near 110 percent of stalling speed. In every instance the pilots reported the airplane tended to roll to the right near the stall with an appreciable loss in altitude involved in the recovery from the stall unless the engine afterburners were used. The pilots also considered the stabilizer effective in the stall recovery. The ailerons, however, were considered only marginally effective.

Static Directional and Lateral Stability Characteristics

Static directional and lateral stability characteristics are presented in figure 15 where the control positions, control forces, and side-force coefficient are plotted as functions of sideslip angle. The

apparent control-fixed directional stability, as shown by the variation of rudder position with sideslip angle, is positive for the narrow speed range covered and increases with increase in Mach number. The data also indicate a smaller degree of stability near zero sideslip angle than at moderate sideslip angles. (The wind-tunnel data of ref. 5 indicate a similar trend of directional stability over the range of sideslip angle at $M = 0.9$.) The value of the apparent stability parameter $d\delta_r/d\beta$ (measured near $\beta = 0^\circ$) increases from 1.15 to 1.60 as the Mach number increases from 0.84 to 0.98.

Figure 15 shows the variation of side-force coefficient with sideslip angle to be linear for each of the three Mach numbers at which the sideslips were performed. However, the previously mentioned increase in apparent stability for moderate angles of sideslip is not reflected in the side-force-coefficient curve. This condition indicates either greater control effectiveness for small values of β and δ_r or a change in fuselage load distribution occurring at moderate values of β, or both. This change in fuselage load distribution would tend to change the linearity of the unstable fuselage moments with increase in β with no accompanying change in fuselage load. The rudder-free directional stability, apparent to the pilot as variation of rudder pedal force with sideslip angle, is positive and approximately linear for a Mach number of 0.84 (fig. 15(a)). For Mach numbers of 0.96 and 0.98, figures 15(b) and 15(c) show an extreme rudder-force—sideslip-angle gradient $dF_r/d\beta$ beyond small values of β. At these higher speeds and at the larger values of β and δ_r the available hydraulic force applied to the rudder is insufficient to overcome the increased rudder hinge moment. Consequently, the increased pedal force does not produce a corresponding increase in rudder deflection and the increased gradient of $dF_r/d\beta$ becomes apparent to the pilot as an increase in rudder-free stability.

The apparent effective dihedral $d\delta_a/d\beta$ as shown by the slope of the curve of aileron position plotted as a function of sideslip angle, is positive for Mach numbers of 0.84 and 0.98 (figs. 15(a) and 15(c)). The near neutral $d\delta_a/d\beta$ slope at $M = 0.96$ (fig. 15(b)) cannot be explained until additional flight test data are available to define the variation of apparent effective dihedral with Mach number.

Since sufficient data are not available to graphically present lateral and directional stability parameters as a function of Mach number, the following table has been included:

Lateral and Directional Stability Characteristics				
M	h_p, ft	$d\delta_r/d\beta$ ($\beta = 0^\circ$)	C_{Y_β} ($\beta = 0^\circ$)	$d\delta_a/d\beta$ ($\beta = 0^\circ$)
0.84	20,000	1.15	-0.0110	0.64
.96	21,000	1.20	-.0115	.08
.98	19,800	1.60	-.0120	.40

Lateral Control Characteristics

The effectiveness of the ailerons over the aileron deflection range and over a very limited Mach number range is shown in figure 16. The relative effectiveness of the ailerons, in terms of the parameter $pb/2V/\delta_a$, appears to be about the same over the Mach number range tested $\left(\frac{pb/2V}{\delta_a} \approx 0.0018\right)$. In addition, the meager data obtained up to this time indicate that the effectiveness of the ailerons appears to be linear with deflection except possibly at $M = 0.94$ where a lower effectiveness may exist for small deflections than for large deflections.

CONCLUSIONS

Results from demonstration tests of the Douglas X-3 airplane by the manufacturer and the U. S. Air Force indicate the following conclusions:

1. Longitudinal control deflection required to trim the airplane exhibited a stable trend over the Mach number range from 0.60 to about 0.92, appeared neutrally stable between Mach numbers of 0.92 and about 0.97, and exhibited a slight nose-down trim change starting at a Mach number of about 1.07 up to 1.16, the highest Mach number at which trim data were obtained.

2. Throughout the Mach number range from 0.65 to 1.21, the apparent static longitudinal stability was positive at low lifts and the apparent stability parameter di_t/dC_{N_A} had a constant value of about -5° for Mach numbers below 0.9 and then increased linearly to -12° at a Mach number of 1.21. The apparent stability exhibited a gradual decrease as lift increased and mild pitch-ups occurred at Mach numbers above 0.95. The

pitch-ups occurred at normal-force coefficients of about 0.7 to 0.8, which is slightly below maximum wing lift at a Mach number of approximately 0.95 and about 0.4 to 0.3 below maximum wing lift at Mach numbers greater than 1.0.

3. Difficulty was experienced in performing smooth longitudinal maneuvers. This effect appeared to result from the combination of control system, airplane, pilot, and their dynamic characteristics; however, additional tests are required to determine the primary cause of the lag and oscillations experienced.

4. Unaccelerated stalls appeared stable in all configurations tested, except at large angles of attack in the landing configuration where some instability was evident. Roll-off tendencies, which became more severe as the speed was decreased, were apparent in all configurations.

5. The airplane normal-force-coefficient-curve slope $C_{N_{A_\alpha}}$ increased from a value of 0.075 to approximately 0.105 as the Mach number increased from 0.65 to 1.0, then decreased to about 0.095 at a Mach number of 1.21.

6. Apparent directional stability over a Mach number range from 0.84 to 0.98 was positive and increased with increase in Mach number. A smaller degree of apparent stability existed for small angles of sideslip than existed at larger angles. Side-force coefficient and effective dihedral were positive for the narrow Mach number range covered.

7. Aileron control effectiveness over a Mach number range of 0.89 to 0.98 was generally linear with deflection and exhibited little change with increase in Mach number.

8. Comparisons showed that flight data, rocket-model data, and wind-tunnel-model data exhibited similar trends and good quantitative agreement.

High-Speed Flight Station,
National Advisory Committee for Aeronautics,
Edwards, Calif., April 25, 1955.

REFERENCES

1. Bellman, Donald R., and Murphy, Edward D.: Lift and Drag Characteristics of the Douglas X-3 Research Airplane Obtained During Demonstration Flights to a Mach Number of 1.20. NACA RM H54I17, 1954.

2. Zalovcik, John A.: A Radar Method of Calibrating Airspeed Installations on Airplanes in Maneuvers at High Altitudes and at Transonic and Supersonic Speeds. NACA Rep. 985, 1950. (Supersedes NACA TN 1979.)

3. Phillips, William H., Brown, B. Porter, and Matthews, James T., Jr.: Review and Investigation of Unsatisfactory Control Characteristics Involving Instability of Pilot-Airplane Combination and Methods for Predicting These Difficulties From Ground Tests. NACA RM L53F17a, 1953.

4. Peck, Robert F., and Mitchell, Jesse L.: Rocket-Model Investigation of Longitudinal Stability and Drag Characteristics of an Airplane Configuration Having a 60° Delta Wing and a High Unswept Horizontal Tail. NACA RM L52K04a, 1953.

5. Olson, Robert N., and Chubb, Robert S.: Wind-Tunnel Tests of a 1/12-Scale Model of the X-3 Airplane at Subsonic and Supersonic Speeds. NACA RM A51F12, 1951.

6. Peck, Robert F., and Hollinger, James A.: A Rocket-Model Investigation of the Longitudinal Stability, Lift, and Drag Characteristics of the Douglas X-3 Configuration With Horizontal Tail of Aspect Ratio 4.33. NACA RM L53F19a, 1953.

7. McKee, John W., and Riebe, John M.: An Investigation of a 0.16-Scale Model of the Douglas X-3 Airplane to Determine Means of Improving the Low-Speed Longitudinal Stability and Control Characteristics. NACA RM L52H01, 1952.

TABLE I

PHYSICAL CHARACTERISTICS OF THE DOUGLAS X-3 AIRPLANE

Wing:	
Airfoil section	Modified hexagon
Airfoil thickness ratio, percent chord	4.5
Airfoil leading- and trailing-edge angles, deg	8.58
Total area, sq ft	166.50
Span, ft	22.69
Mean aerodynamic chord, ft	7.84
Root chord, ft	10.58
Tip chord, ft	4.11
Taper ratio	0.39
Aspect ratio	3.09
Sweep at 0.75 chord line, deg	0
Incidence, deg	0
Dihedral, deg	0
Geometric twist, deg	0
Aileron:	
Area rearward of hinge line (each), sq ft	4.04
Span at hinge line (each), ft	3.25
Chord rearward of hinge line, percent wing chord	25
Travel (each), deg	±12
Leading-edge flap:	
Type	Plain
Area (each), sq ft	8.38
Span at hinge line (each), ft	8.916
Chord, normal to hinge line, in.	11.50
Travel, deg	30
Trailing-edge flap:	
Type	Split
Area (each), sq ft	8.61
Span, ft	5.083
Chord, percent wing chord	25
Travel, deg	50
Horizontal tail:	
Airfoil section	Modified hexagon
Airfoil thickness ratio at root chord, percent chord	8.01
Airfoil thickness ratio outboard of station 26, percent chord	4.50
Airfoil leading-edge angle, deg	11.96
Airfoil trailing-edge angle, deg	8.77
Total area, sq ft	43.24
Span, ft	13.77
Mean aerodynamic chord, ft	3.34
Root chord, ft	4.475
Tip chord, ft	1.814
Taper ratio	0.405
Aspect ratio	4.38
Sweep at leading edge, deg	21.14
Sweep at trailing edge, deg	0
Dihedral, deg	0

TABLE I

PHYSICAL CHARACTERISTICS OF THE DOUGLAS X-3 AIRPLANE - Concluded

Travel:	
Leading edge up, deg	6
Leading edge down, deg	17
Hinge line location, percent root chord	46.46
Vertical tail:	
Airfoil section	Modified hexagon
Airfoil thickness ratio, percent chord	4.5
Airfoil leading- and trailing-edge angles, deg	8.58
Area, sq ft	23.73
Span (from horizontal tail hinge line), ft	5.59
Mean aerodynamic chord, ft	4.69
Root chord, ft	6.508
Tip chord, ft	1.93
Taper ratio	0.292
Aspect ratio	1.315
Sweep at leading edge, deg	45
Sweep at trailing edge, deg	9.39
Rudder:	
Area, rearward of hinge line, sq ft	5.441
Span at hinge line, ft	3.535
Root chord, ft	1.98
Tip chord, ft	1.097
Travel, deg	±20
Fuselage:	
Length including boom, ft	66.75
Maximum width, ft	6.08
Maximum height, ft	4.81
Base area, sq ft	7.94
Power plant:	
Engines	Two Westinghouse J34-WE-17 with afterburner
Rating, each engine:	
Static sea-level maximum thrust, lb	4,850
Static sea-level military thrust, lb	3,370
Airplane weight, lb:	
Basic (without fuel, oil, water, pilot)	16,120
Total (full fuel, oil, water, no pilot)	21,900
Center-of-gravity location, percent $\bar{c}$:	
Basic weight - gear down	2.63
Total weight - gear down	4.59
Total weight - gear up	3.91

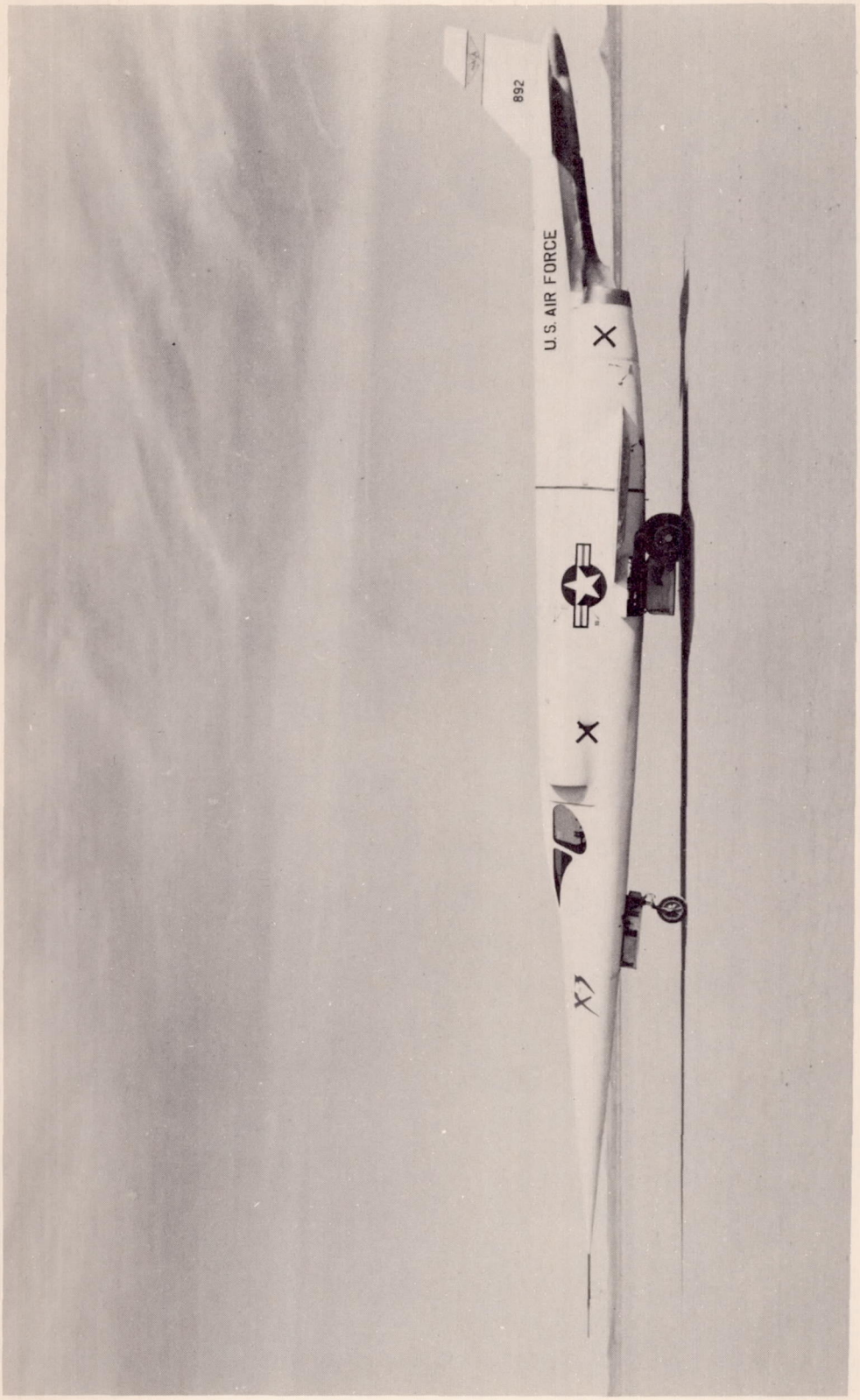

L-87961

Figure 1.- Side view of Douglas X-3 research airplane.

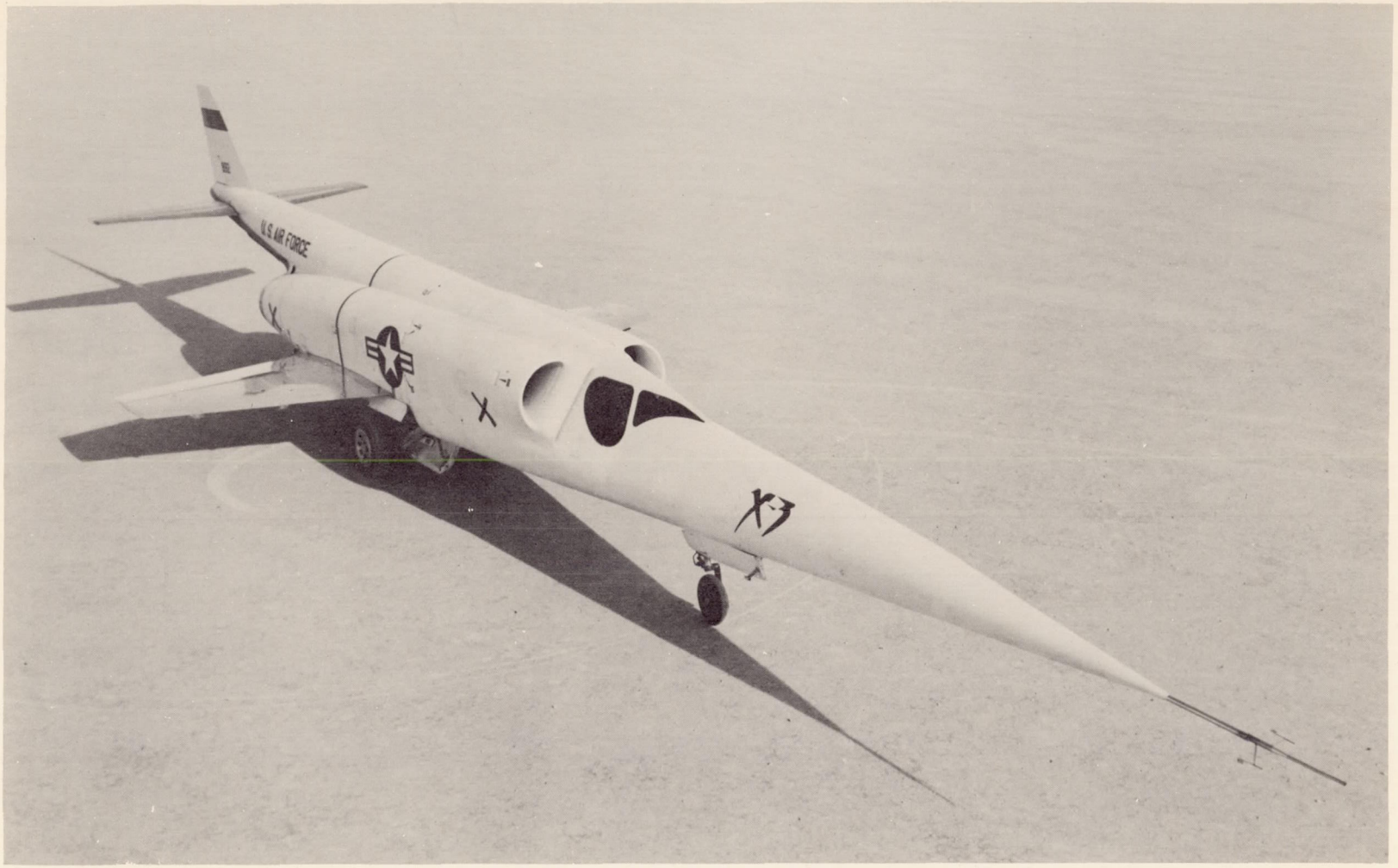

L-87962

Figure 2.- Three-quarter front view of Douglas X-3 research airplane.

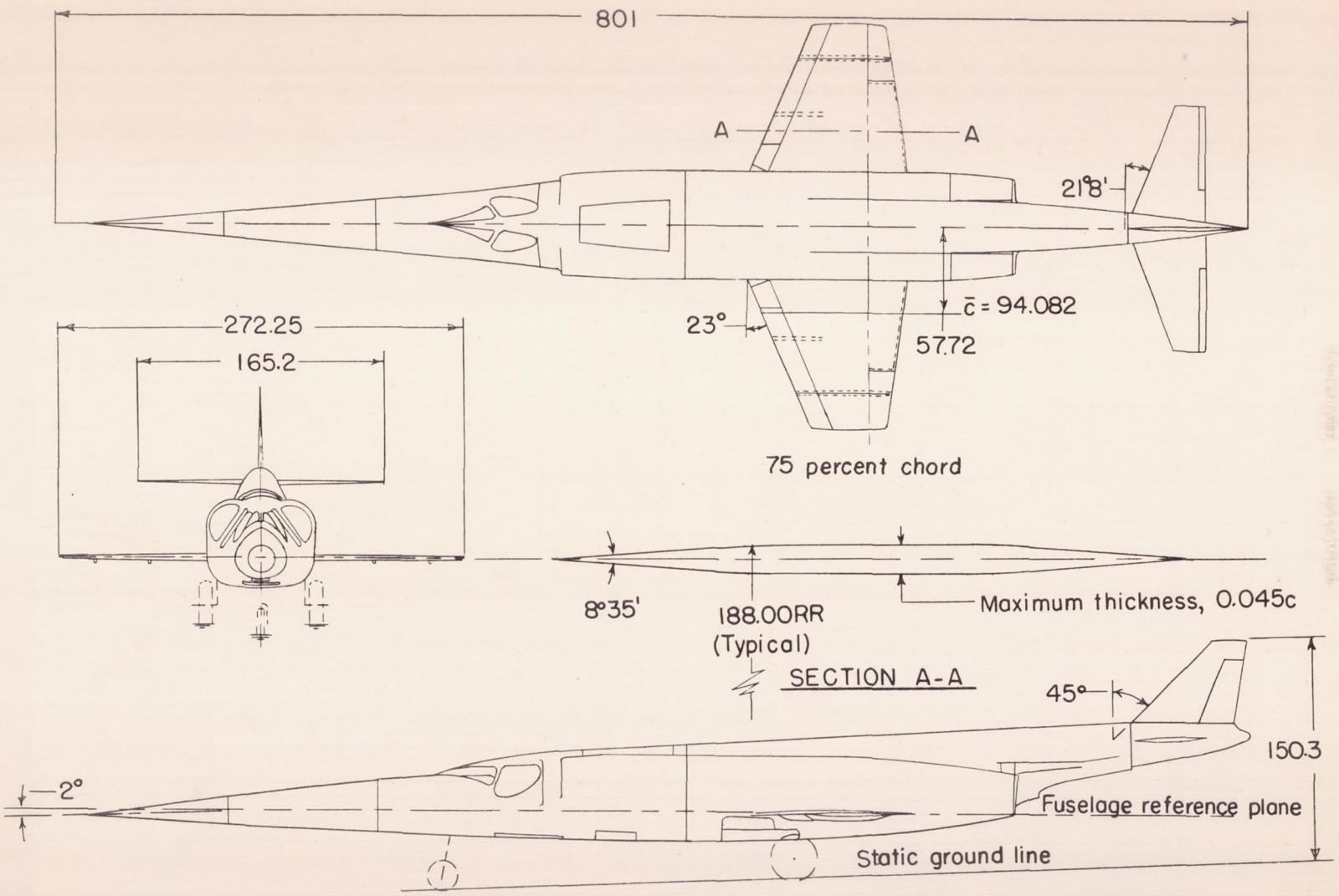

Figure 3.- Three-view drawing of X-3 airplane. All linear dimensions in inches.

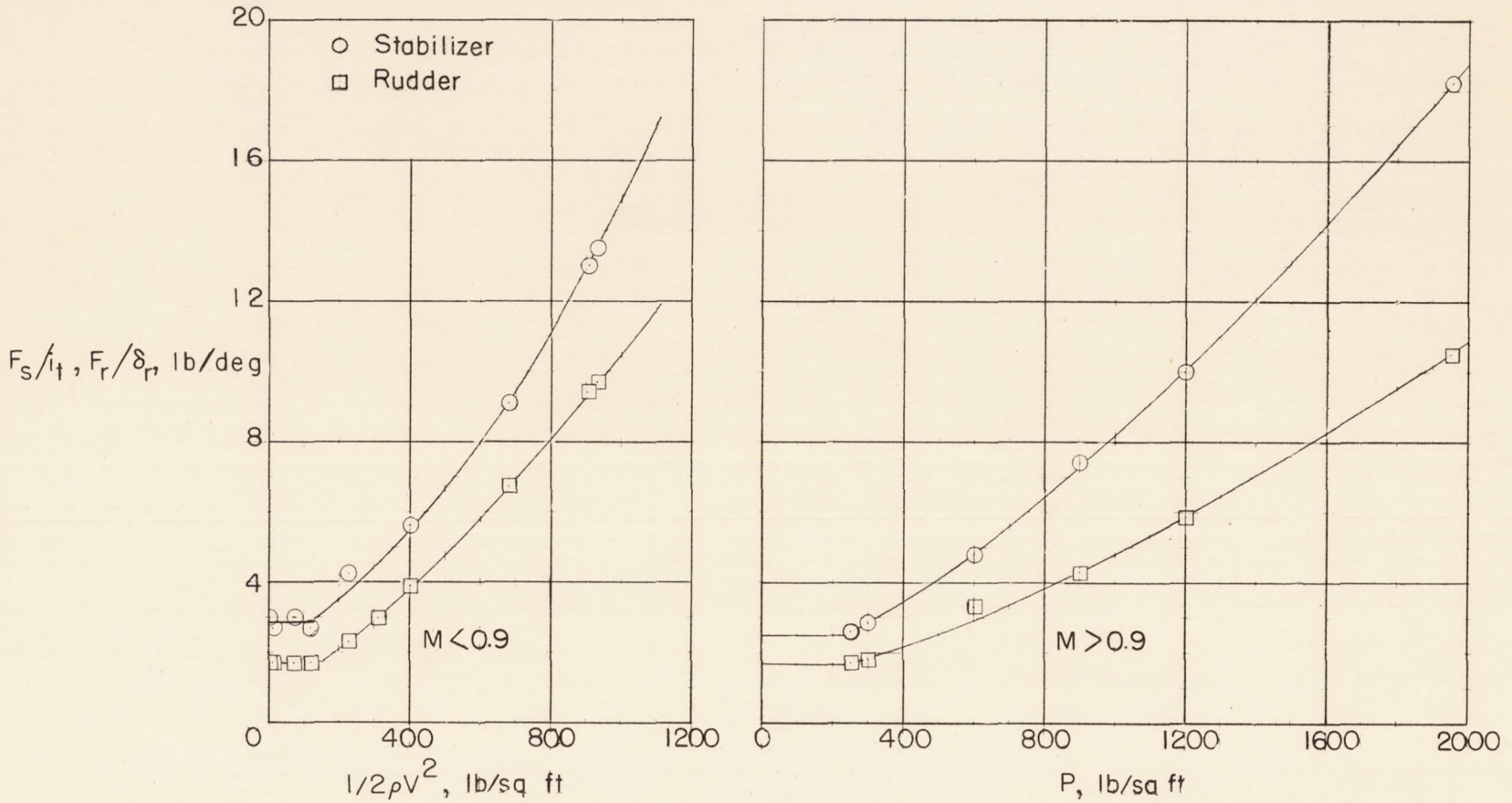

(a) Longitudinal and directional load feel characteristics.

Figure 4.- Synthetic control force characteristics of the Douglas X-3 airplane obtained during ground tests.

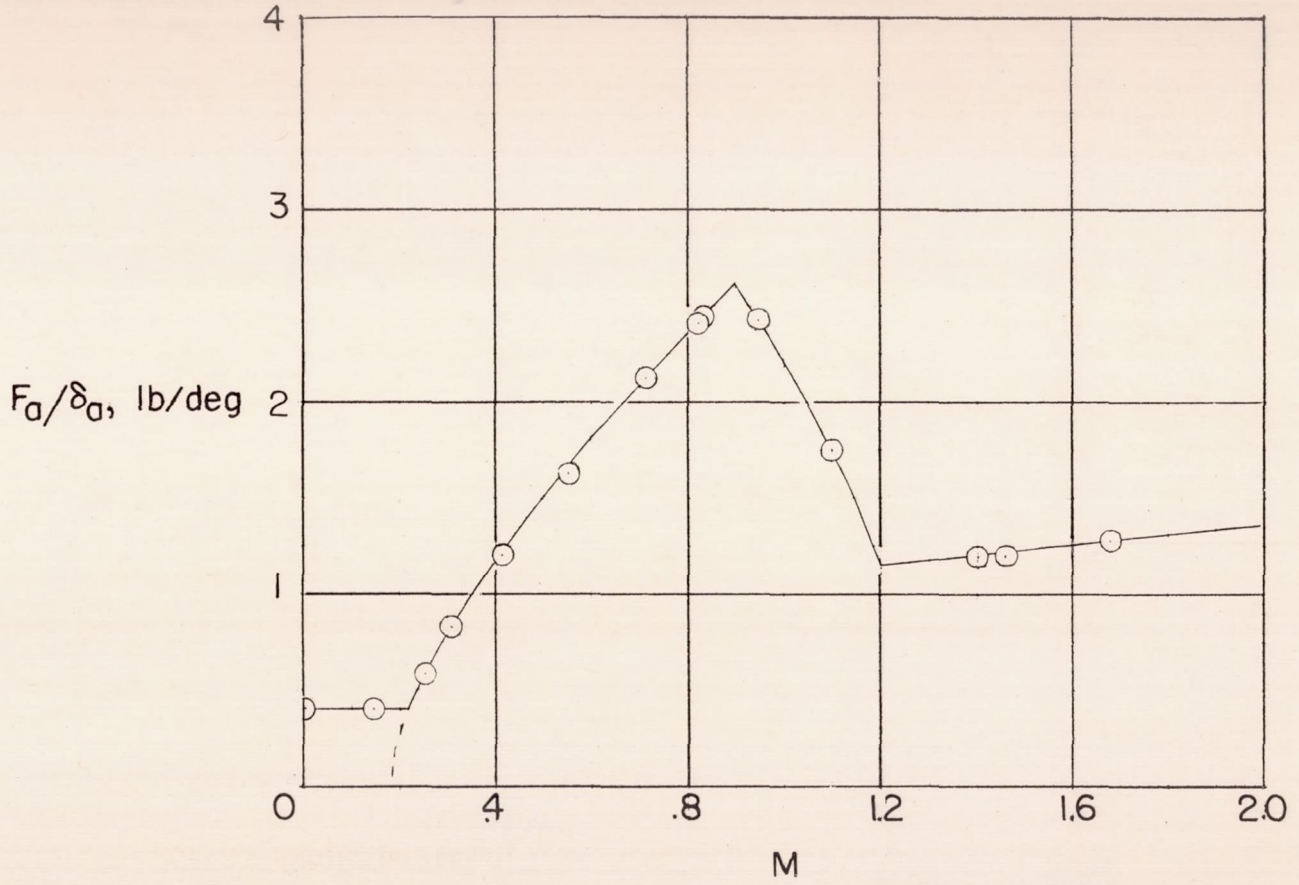

(b) Lateral load feel characteristics.

Figure 4.- Concluded.

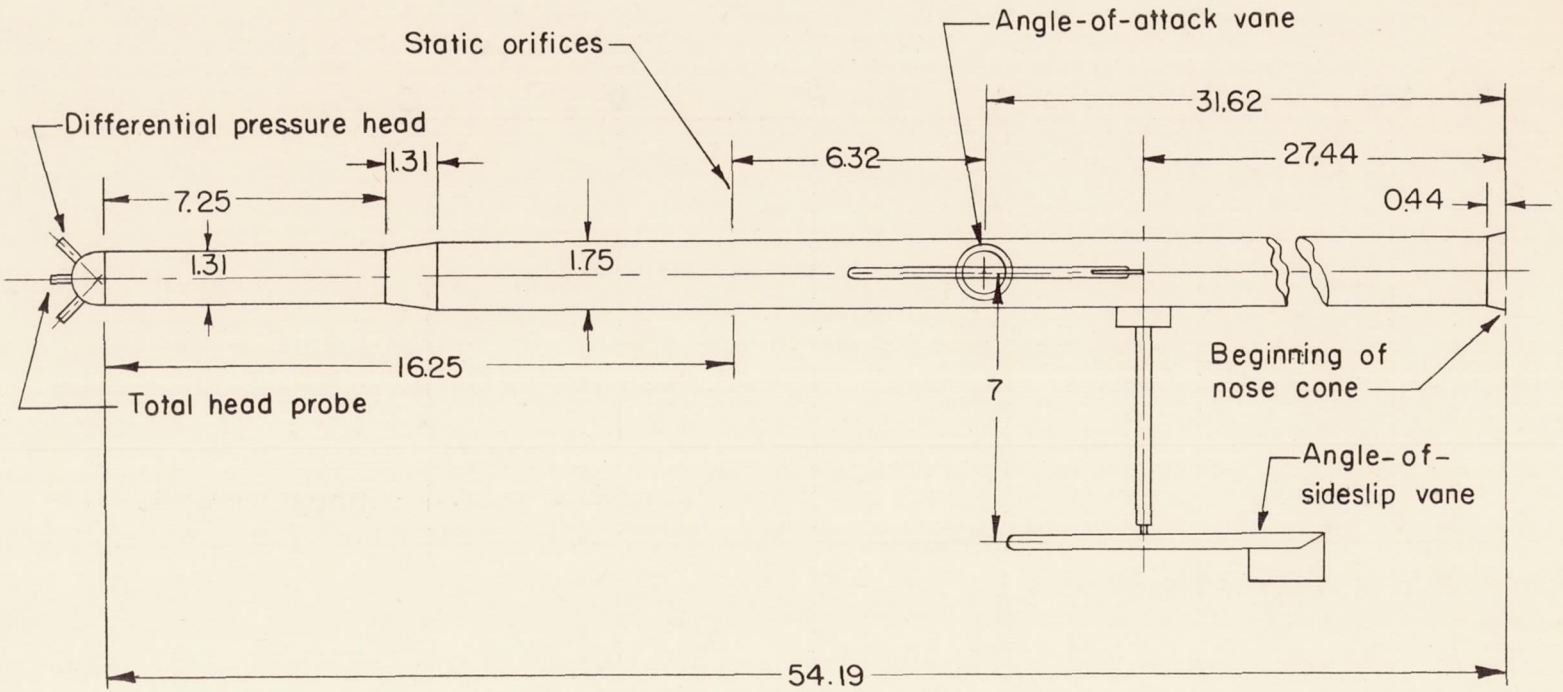

Figure 5.- Sketch of nose boom showing airspeed head and the angle-of-attack and angle-of-sideslip vanes. All dimensions in inches.

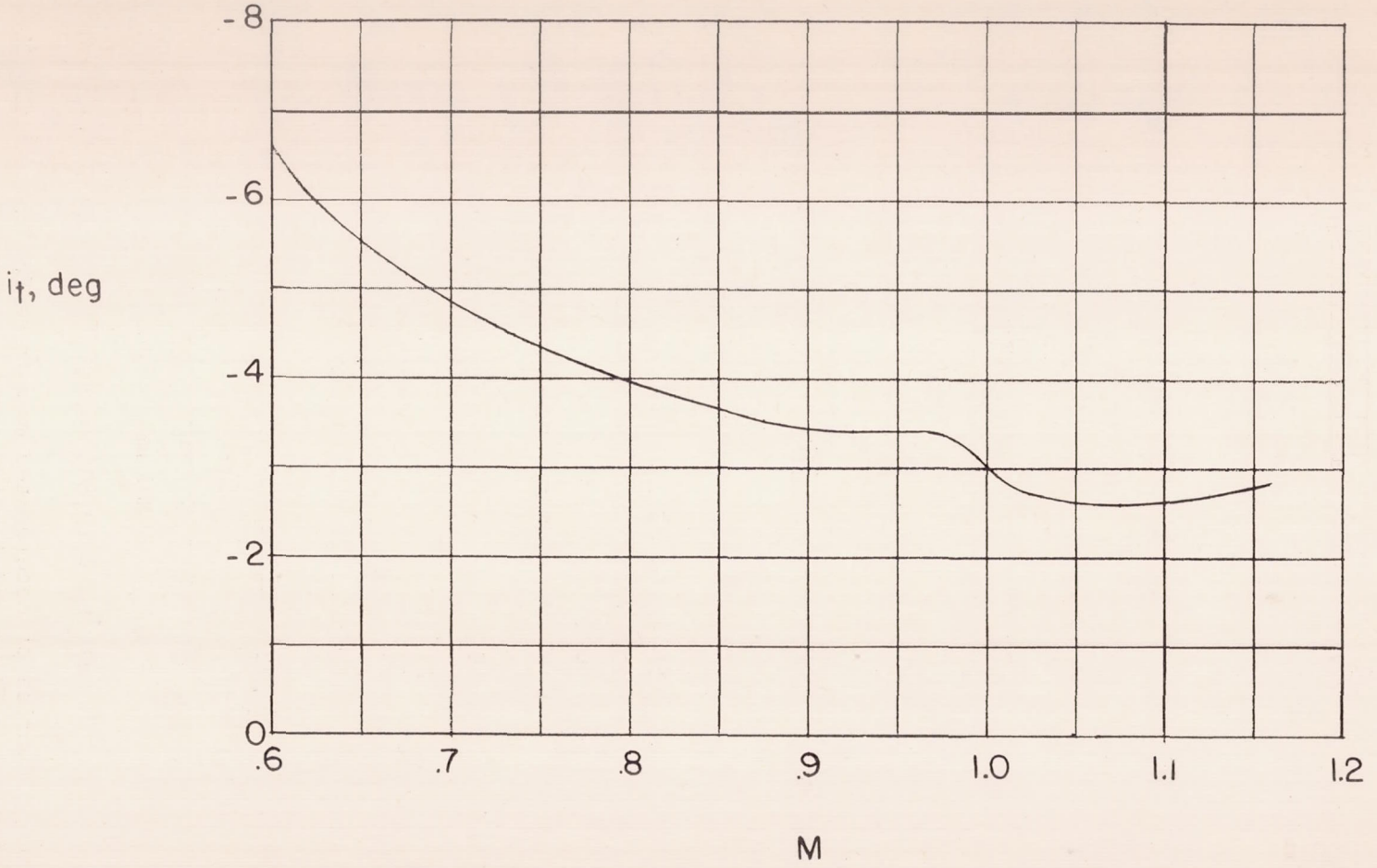

Figure 6.- Stabilizer deflection required for trim as a function of Mach number; clean condition. All data corrected to 1g flight at h_p = 30,000 feet for W/S = 116 lb/sq ft. Douglas X-3 research airplane.

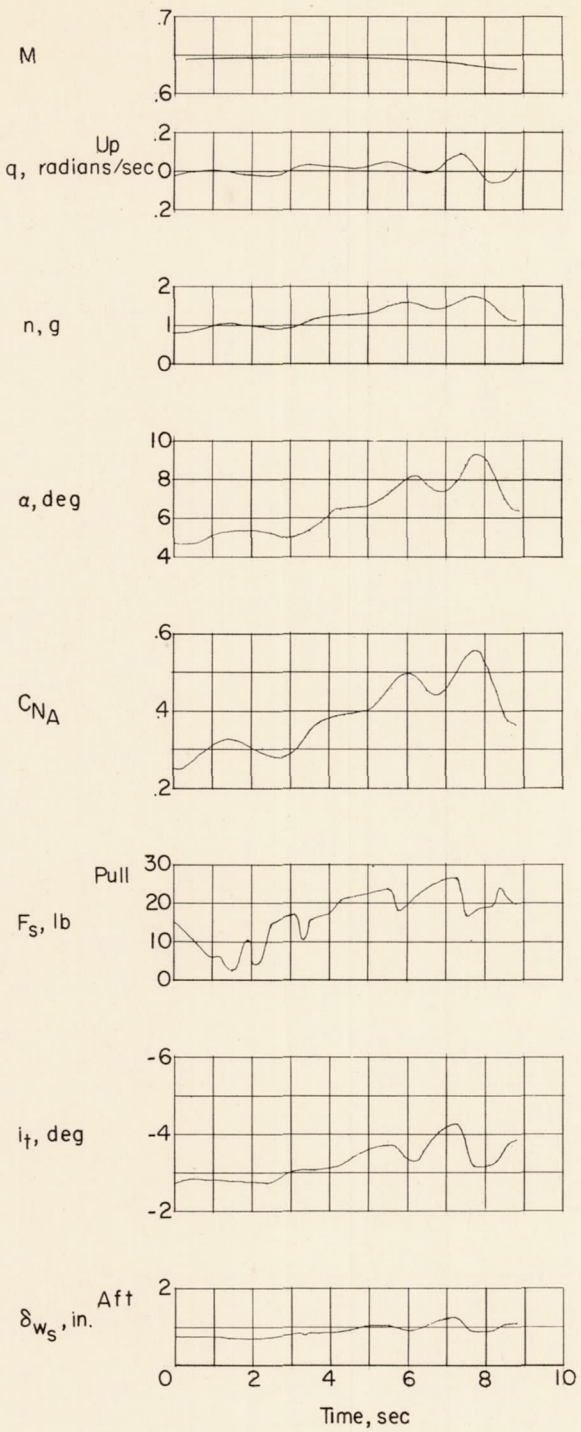

(a) h_p = 12,800 feet.

Figure 7.- Time histories of accelerated maneuvers for the Douglas X-3 research airplane. Flaps and landing gear up; center of gravity from 3 to -2 percent mean aerodynamic chord.

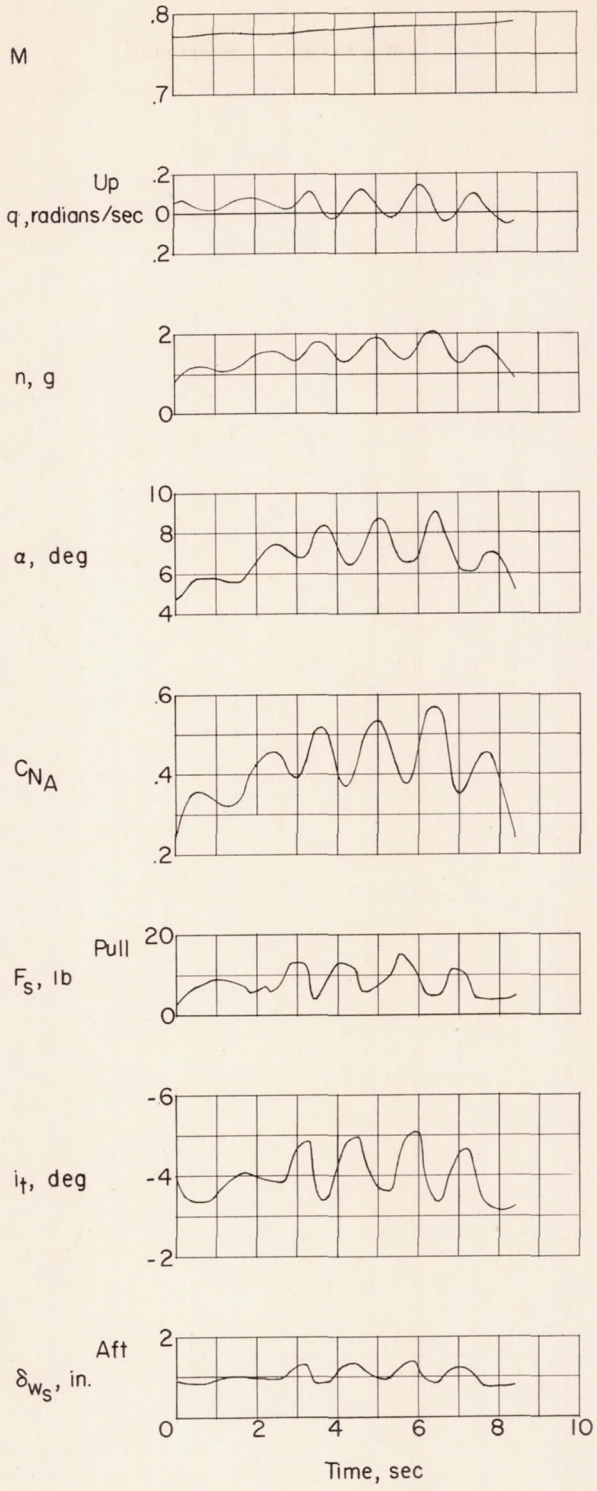

(b) h_p = 22,200 feet.

Figure 7.- Continued.

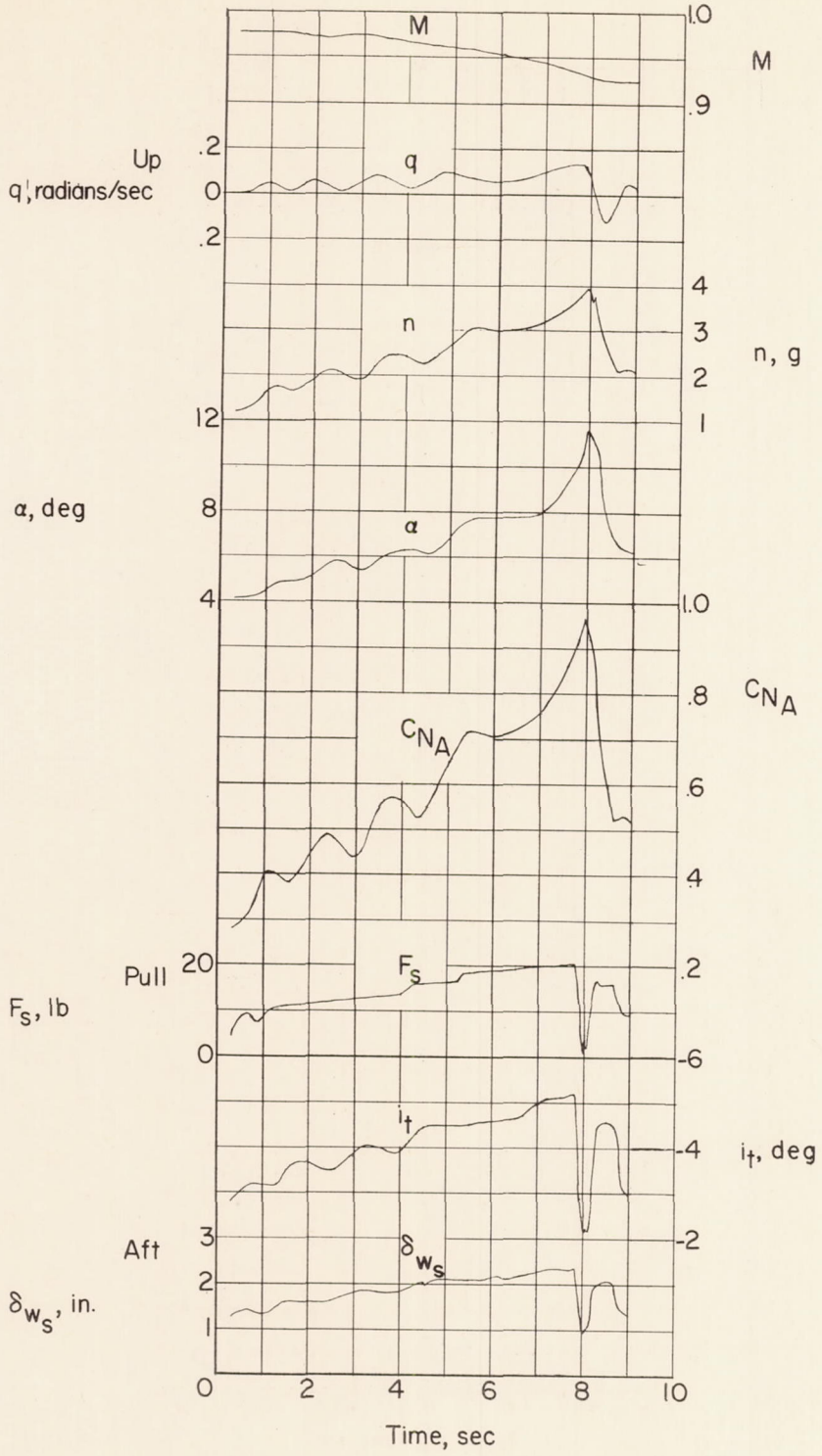

(c) h_p = 25,200 feet.

Figure 7.- Continued.

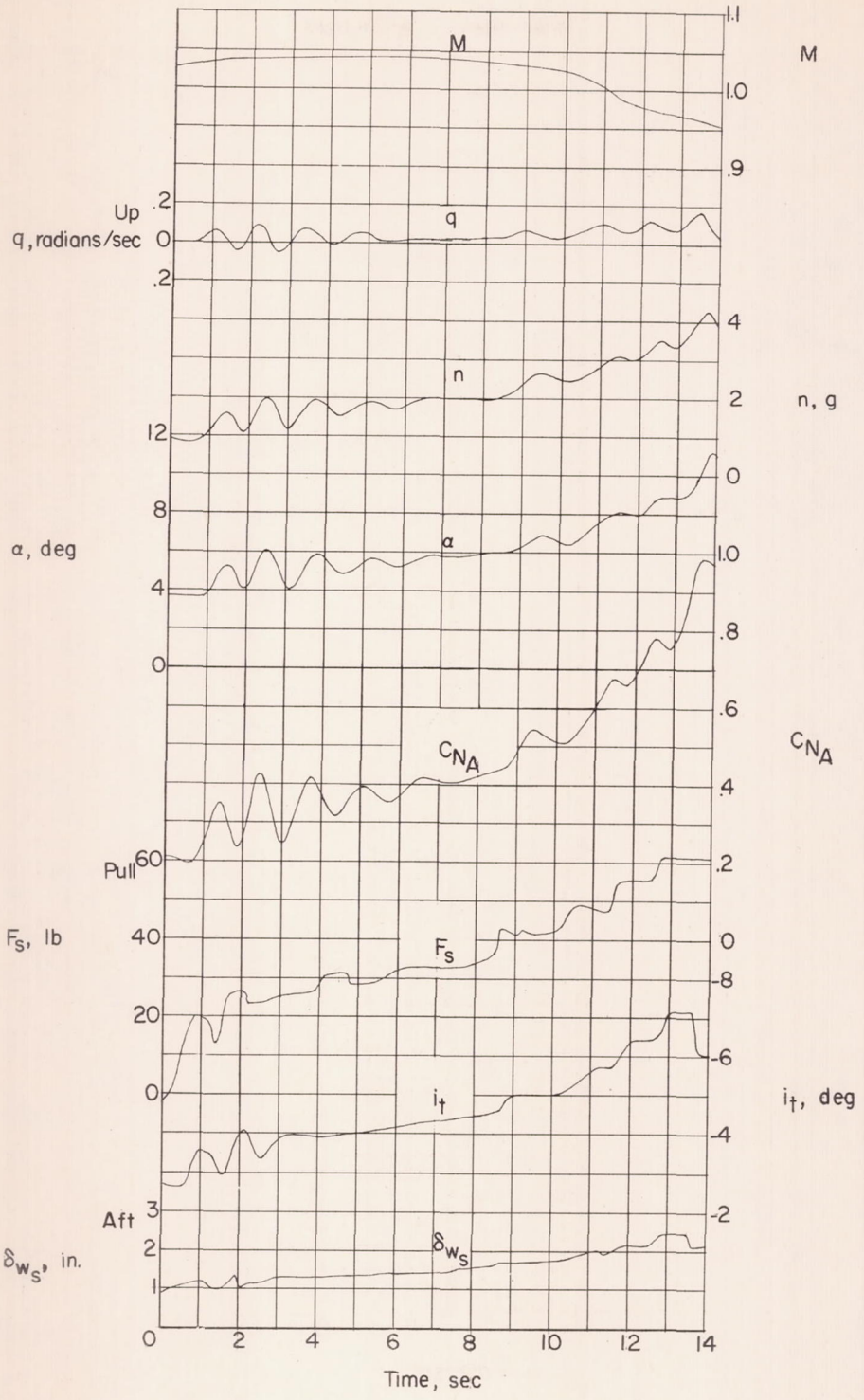

(d) h_p = 26,000 feet.

Figure 7.- Continued.

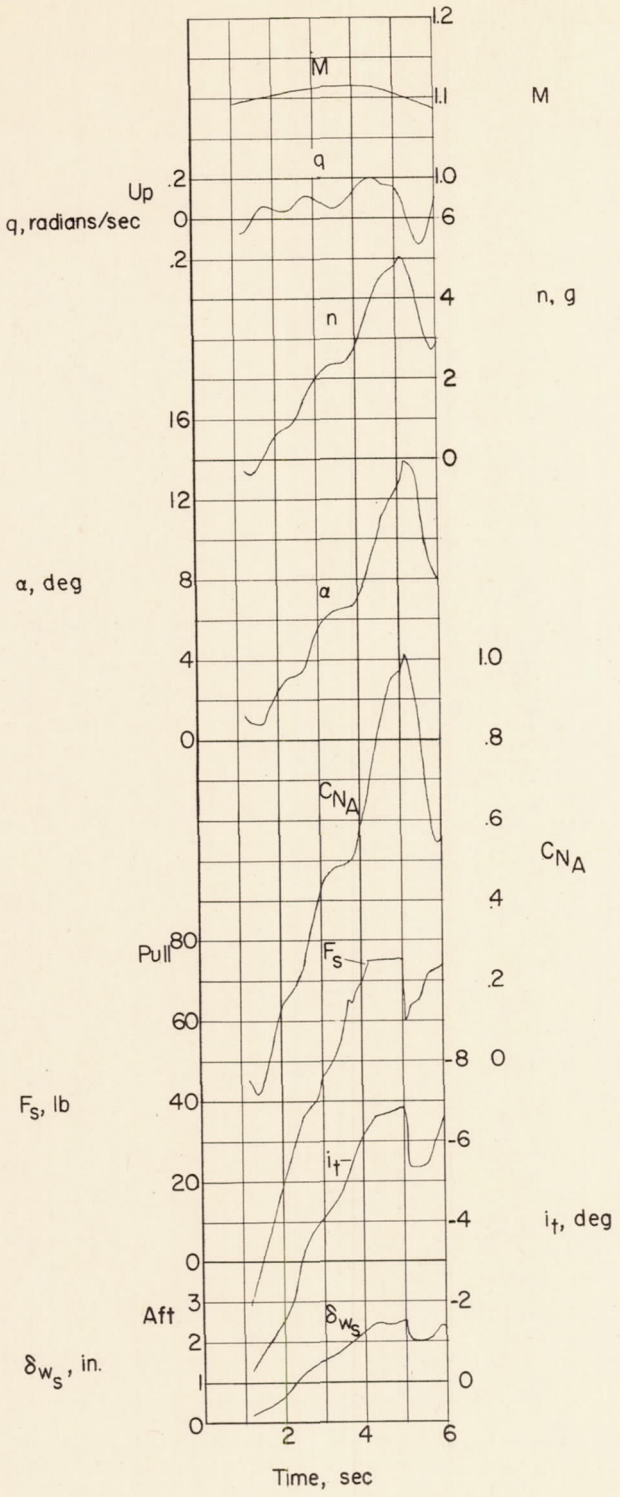

(e) h_p = 28,000 feet.

Figure 7.- Continued.

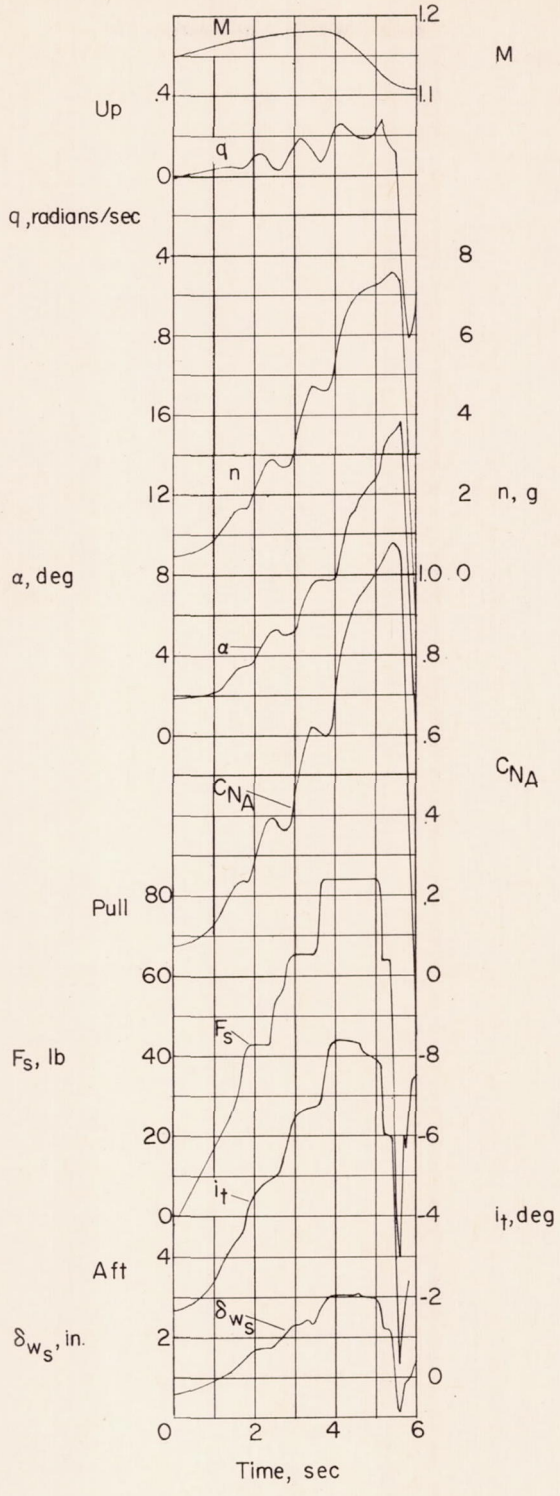

(f) h_p = 22,500 feet.

Figure 7.- Concluded.

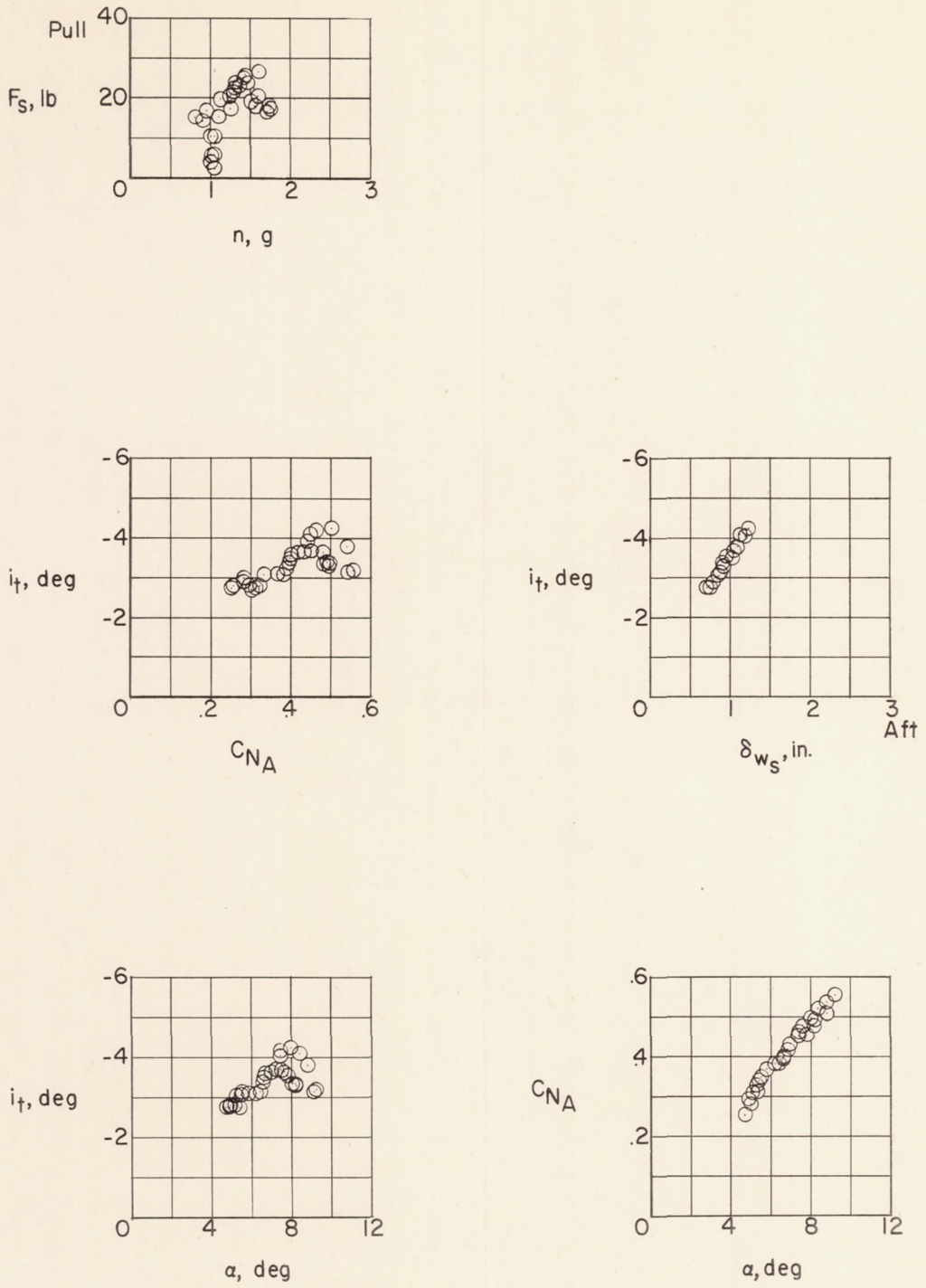

(a) h_p = 12,800 feet; M = 0.645.

Figure 8.- Static longitudinal stability characteristics of Douglas X-3 research airplane in accelerated flight. Flap and landing gear up; center of gravity from 3 to -2 percent mean aerodynamic chord.

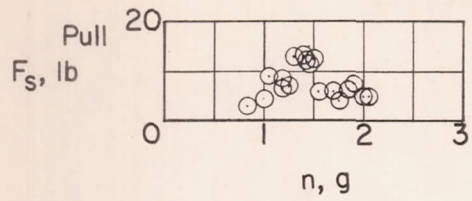

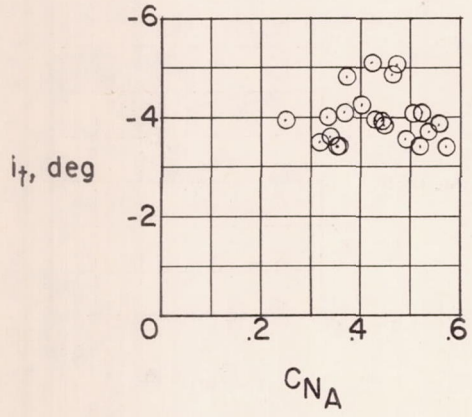

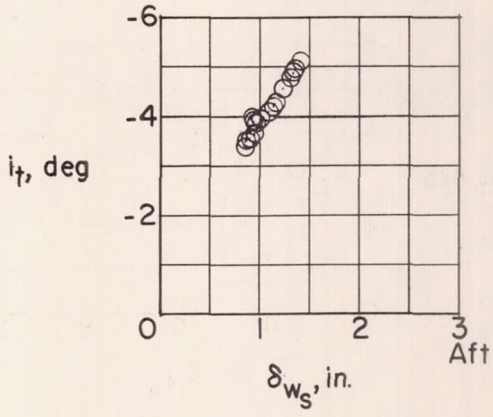

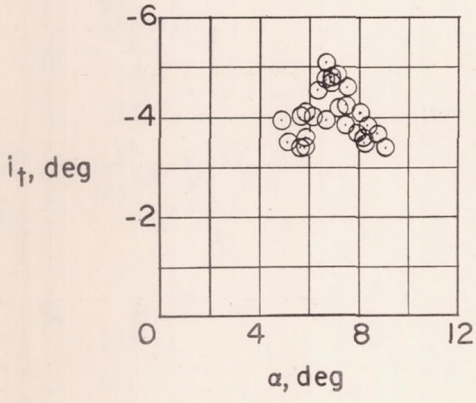

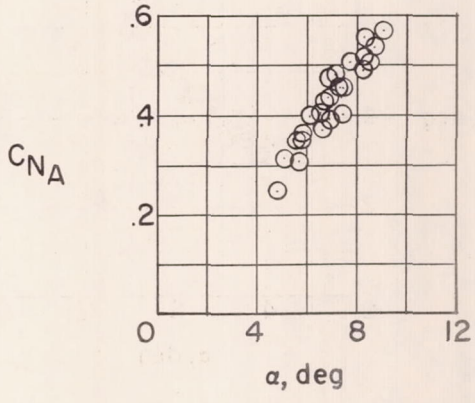

(b) h_p = 22,200 feet; M ≈ 0.78.

Figure 8.- Continued.

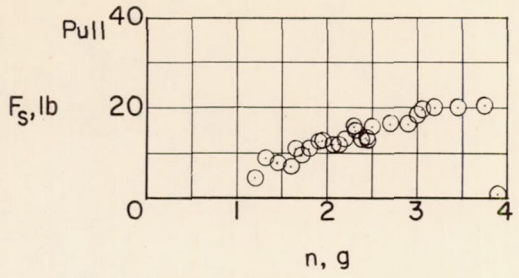

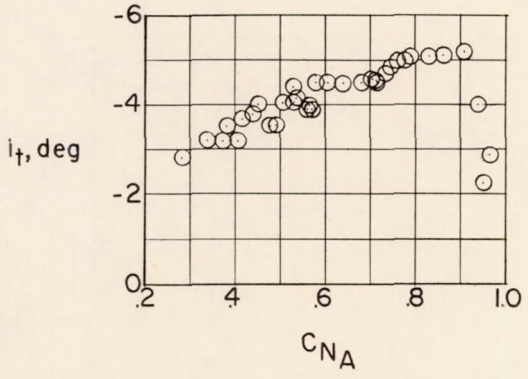

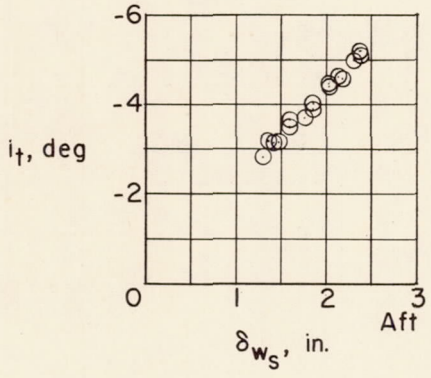

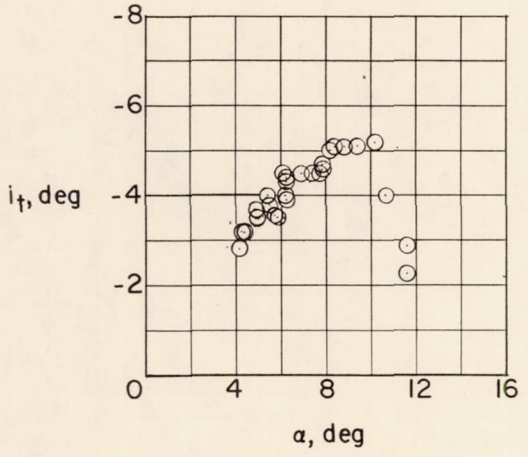

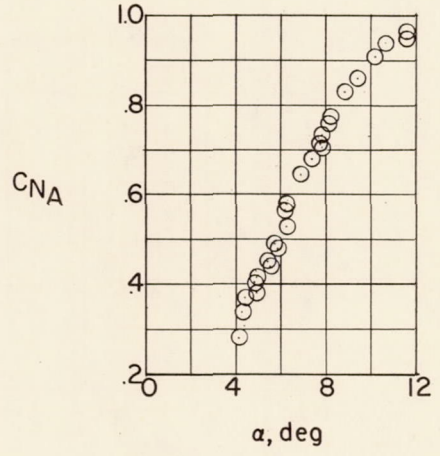

(c) h_p = 25,200 feet; M ≈ 0.97.

Figure 8.- Continued.

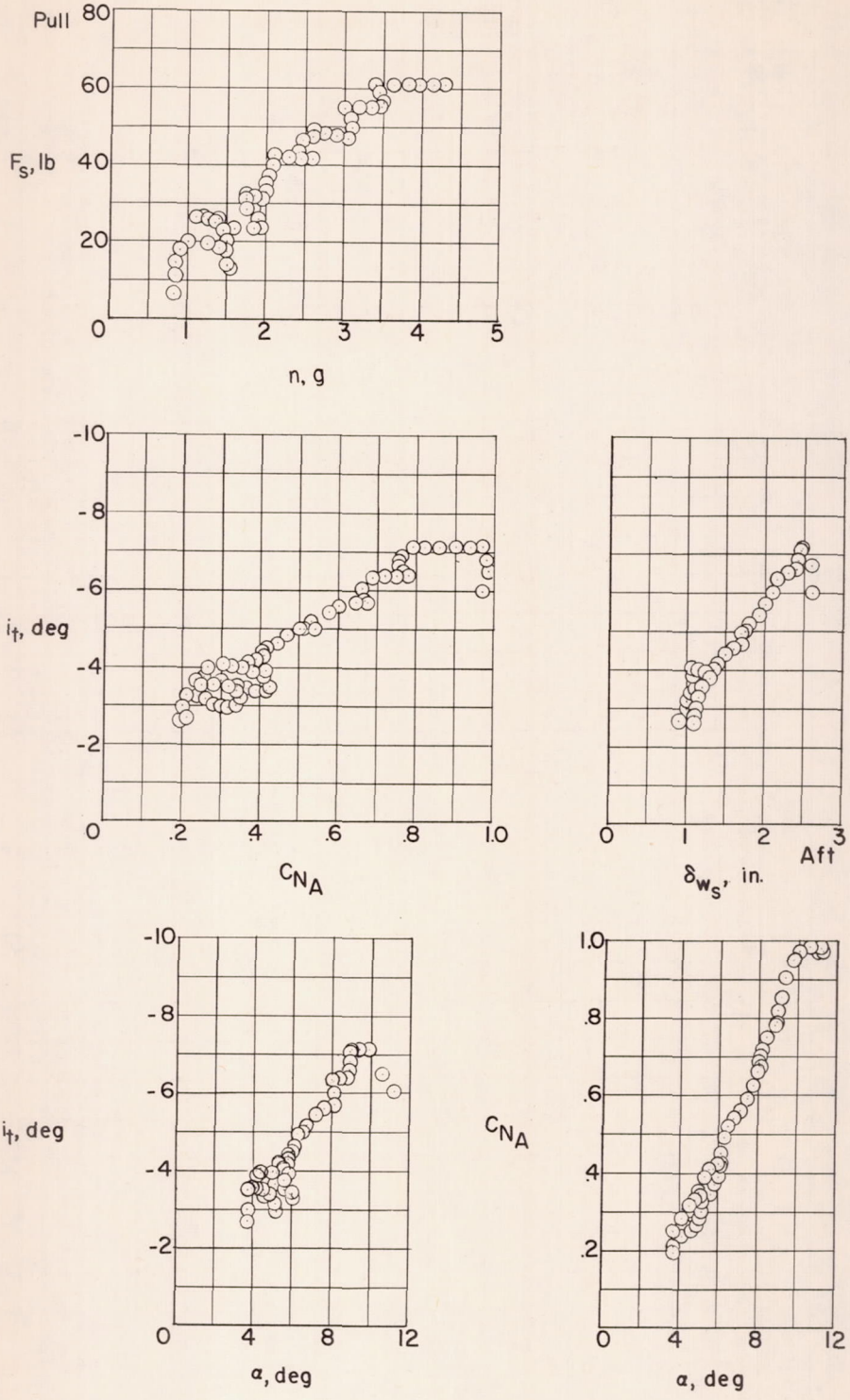

(d) h_p = 26,000 feet; M ≈ 1.04.

Figure 8.- Continued.

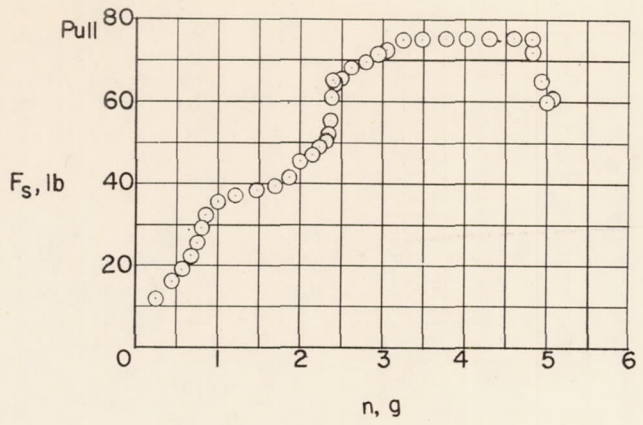

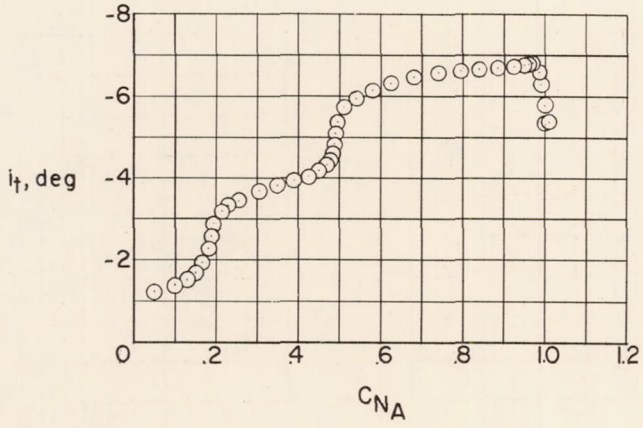

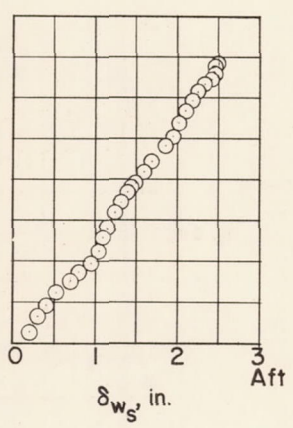

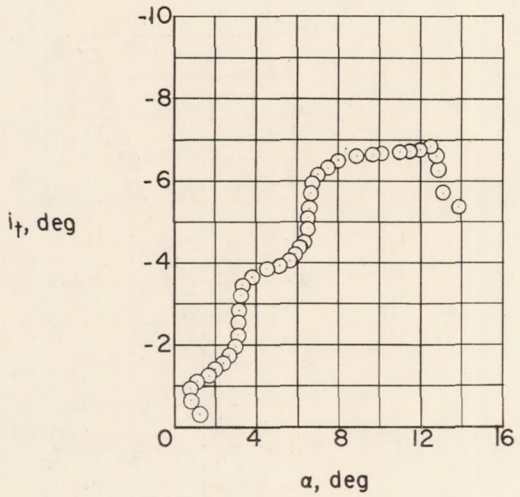

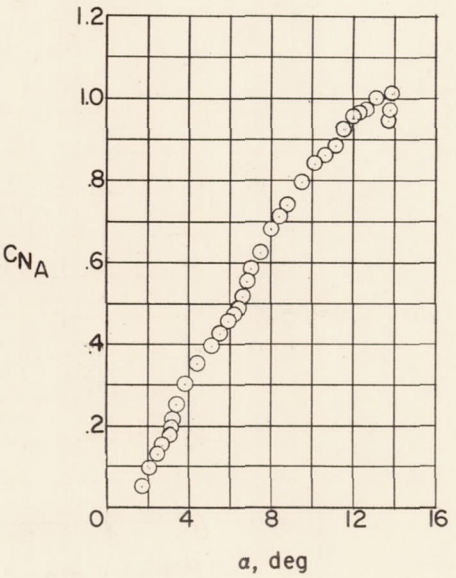

(e) h_p = 28,000 feet; M ≈ 1.11.

Figure 8.- Continued.

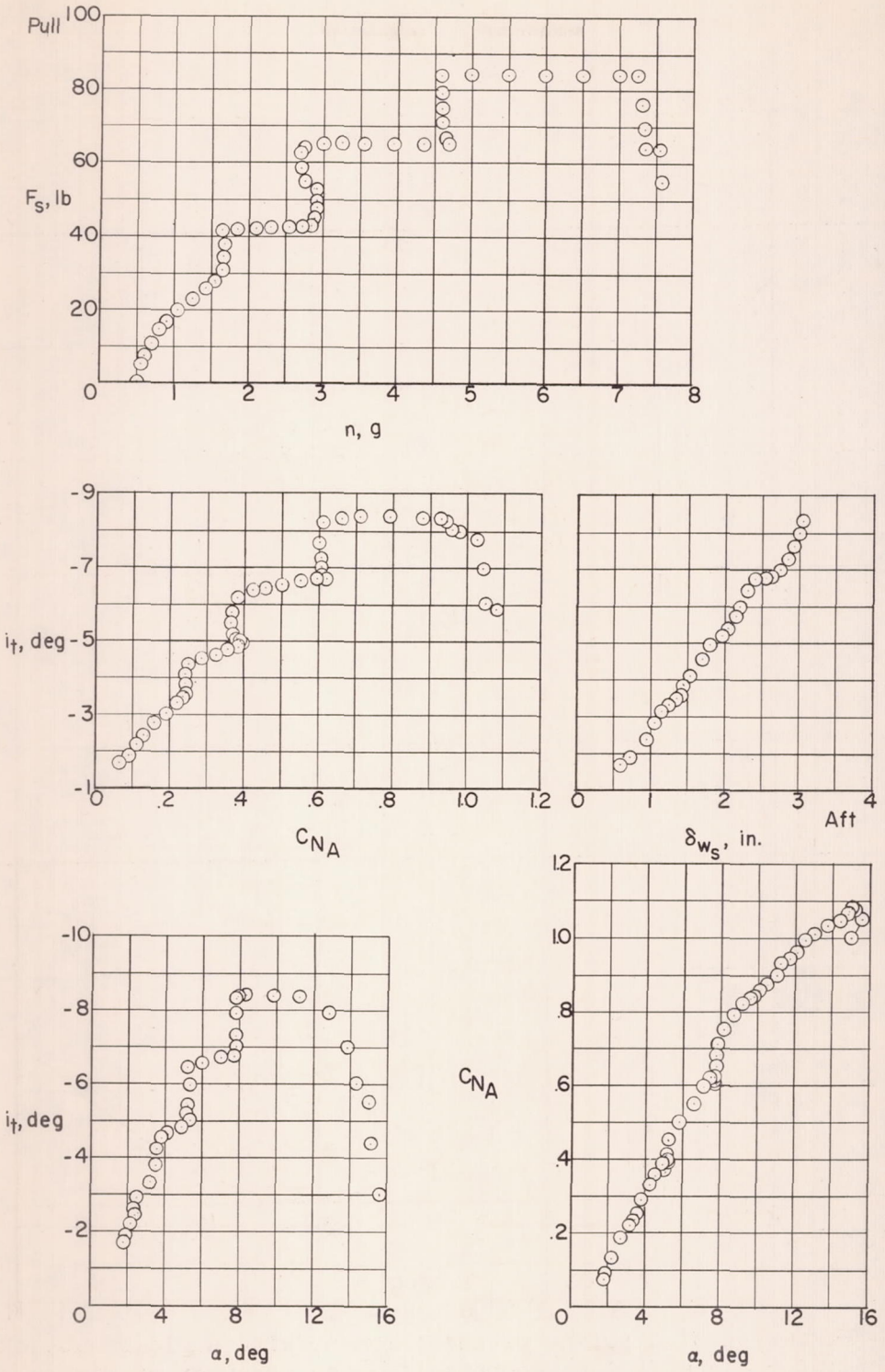

(f) h_p = 22,500 feet; M ≈ 1.17.

Figure 8.- Concluded.

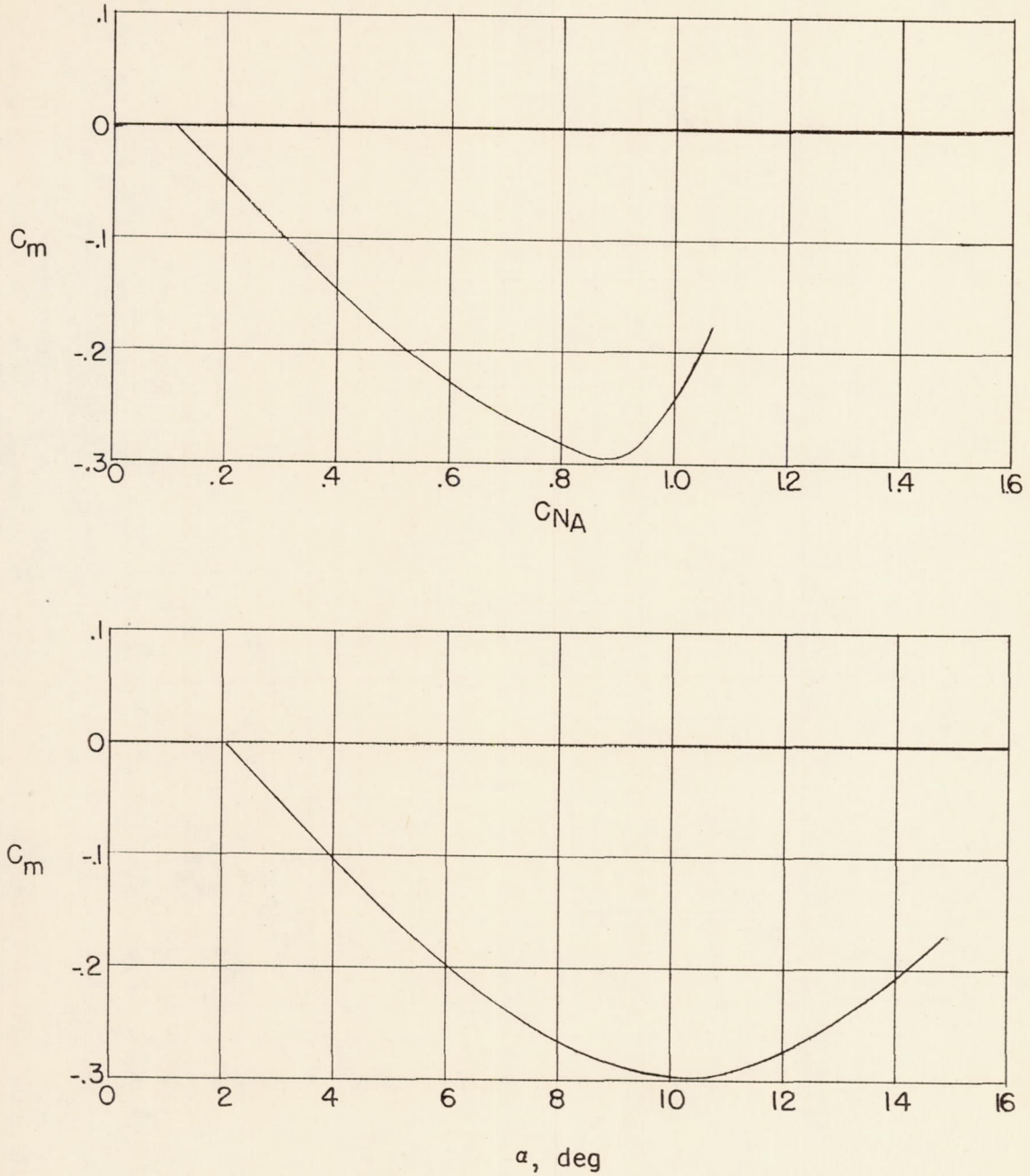

Figure 9.- Variation of airplane pitching moment with angle of attack and normal-force coefficient computed for the maneuver of figure 7(f).

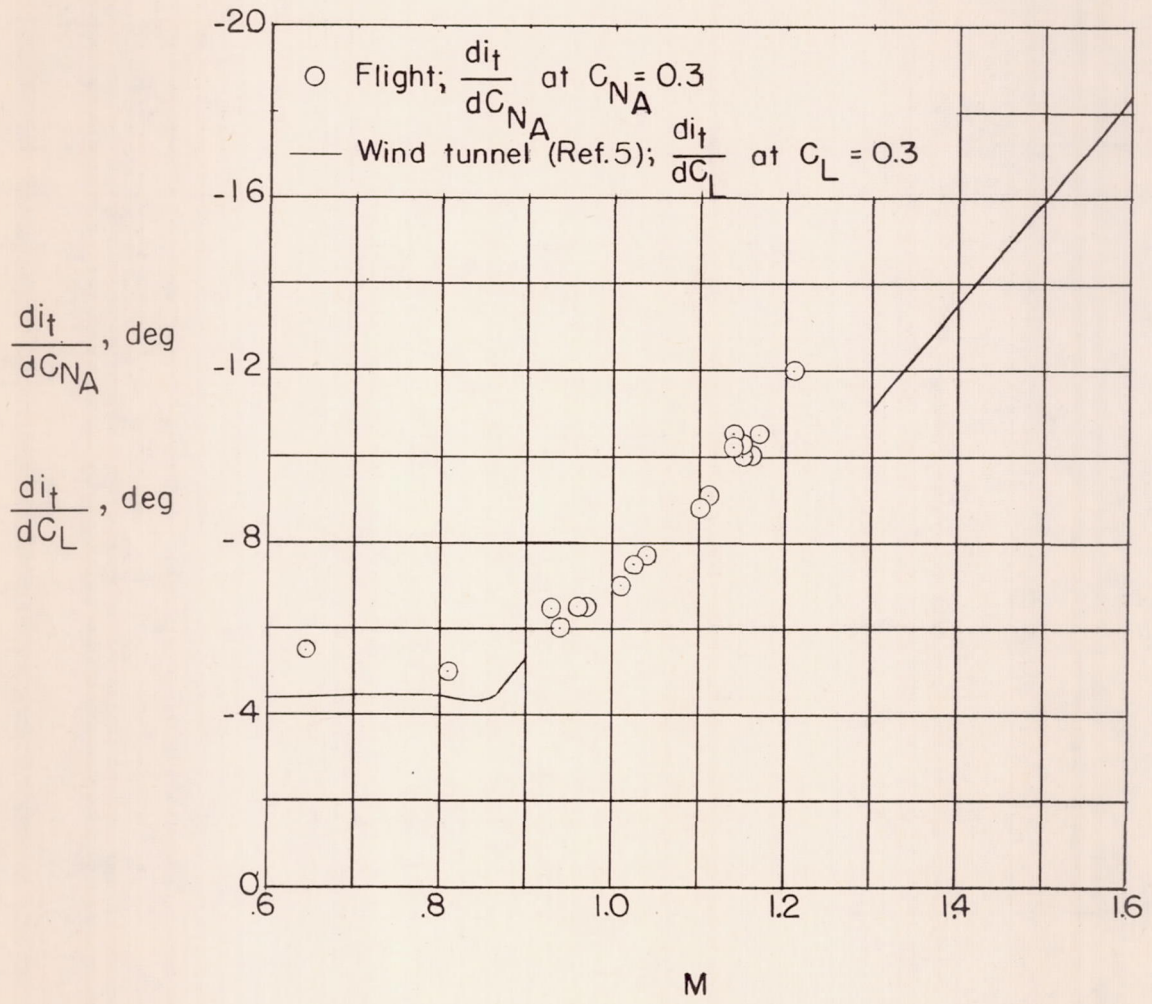

Figure 10.- Variation of $\frac{di_t}{dC_{N_A}}$ with Mach number. Douglas X-3 research airplane.

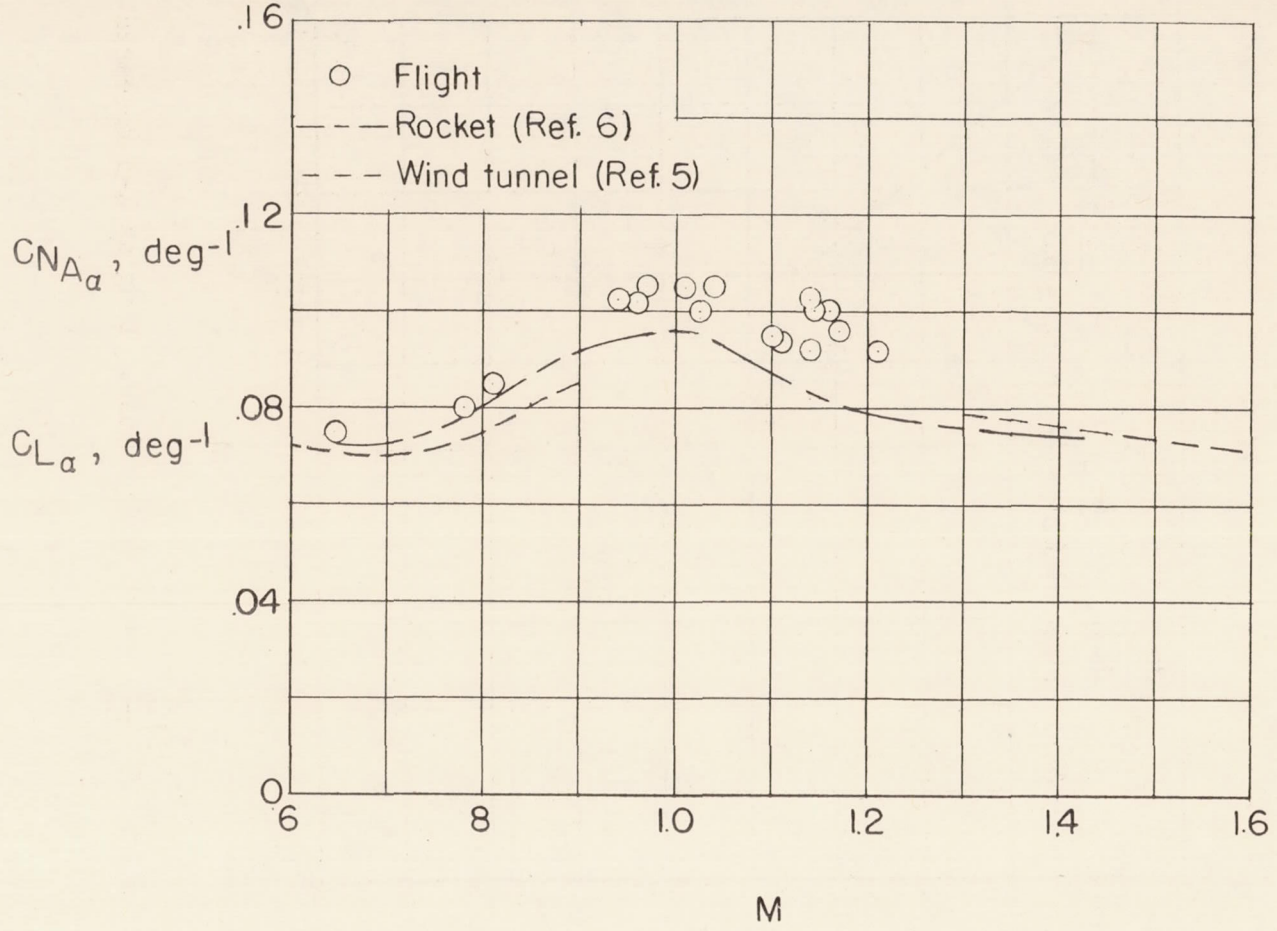

Figure 11.- Variation of airplane normal-force-coefficient-curve slope $C_{N_{A_\alpha}}$ with Mach number. Douglas X-3 research airplane.

(a) Clean configuration.

Figure 12.- Time histories of stall approaches for the Douglas X-3 research airplane; $h_p \approx 26{,}000$ feet; center of gravity from 3 to -2 percent mean aerodynamic chord.

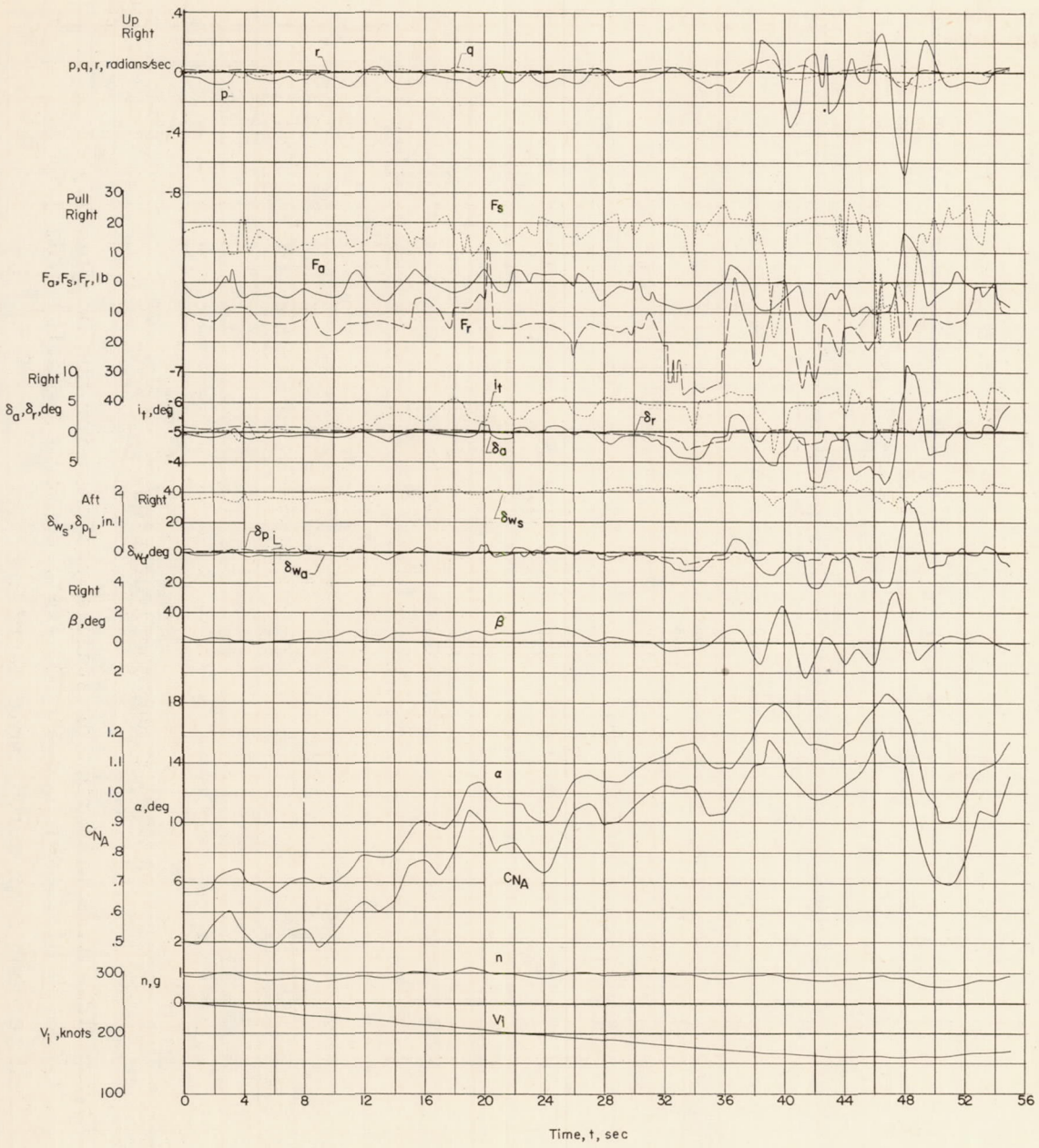

(b) Wheels and flaps extended.

Figure 12.- Continued.

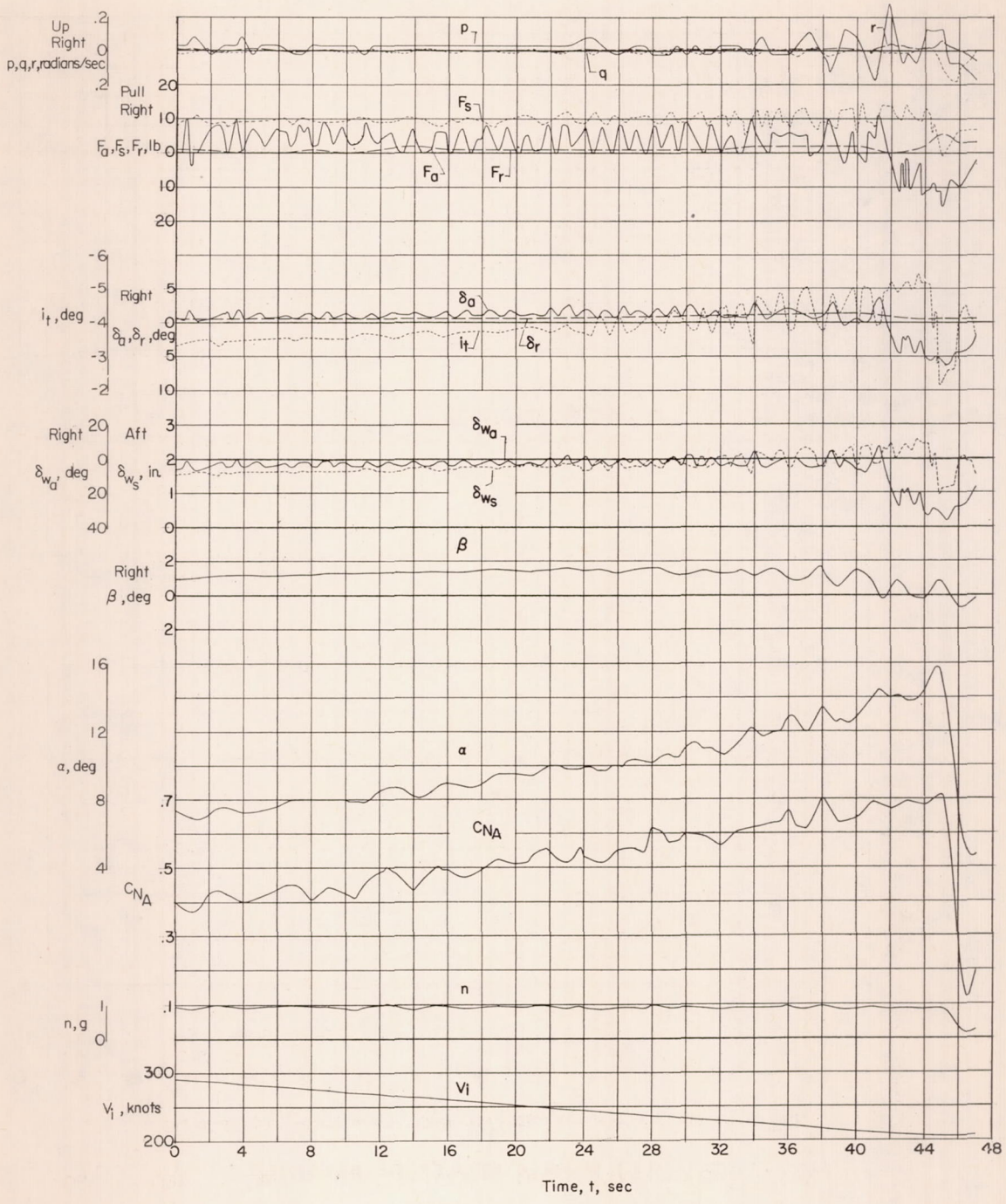

(c) Gear up; $\delta_{f_{te}} = 0$; $\delta_{f_{le}} = 7.0^{\circ}$.

Figure 12.- Concluded.

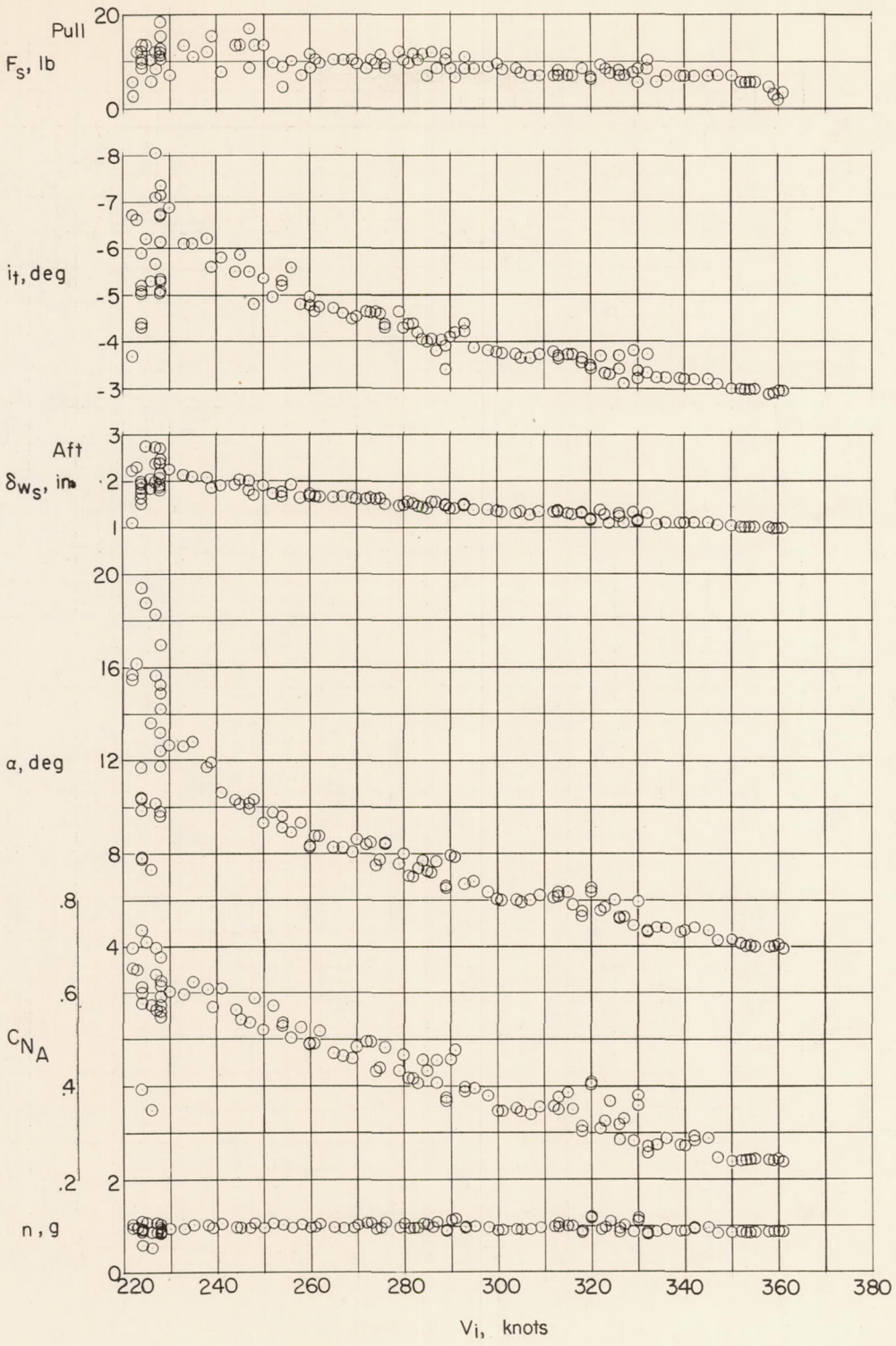

(a) Clean configuration.

Figure 13.- Variation of longitudinal stability and control quantities with indicated airspeed during stall approaches. $h_p \approx 26{,}000$ feet. Douglas X-3 research airplane.

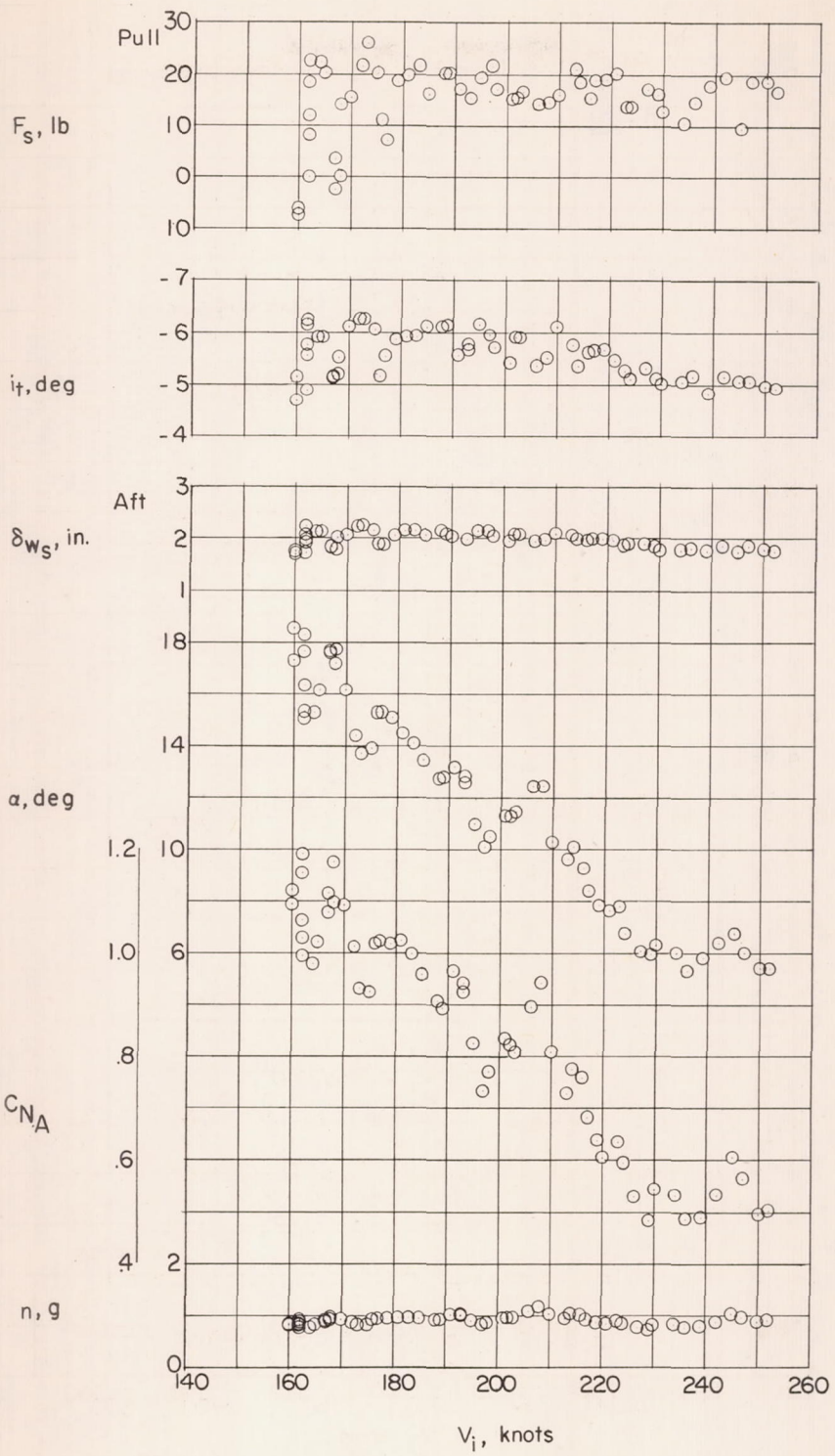

(b) Wheels and flaps extended.

Figure 13.- Continued.

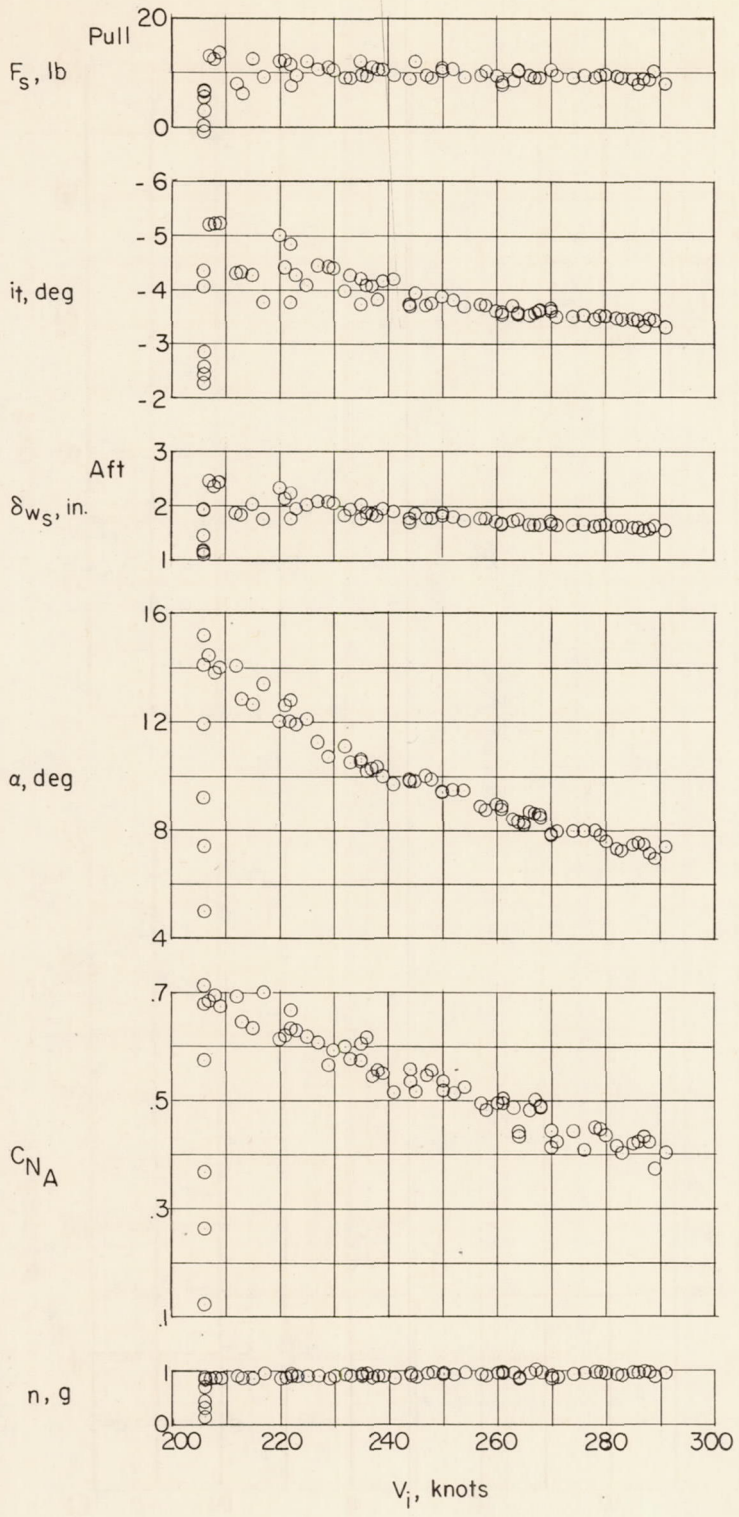

(c) Gear up; $\delta_{f_{te}} = 0$; $\delta_{f_{le}} = 7.0^{\circ}$.

Figure 13.- Concluded.

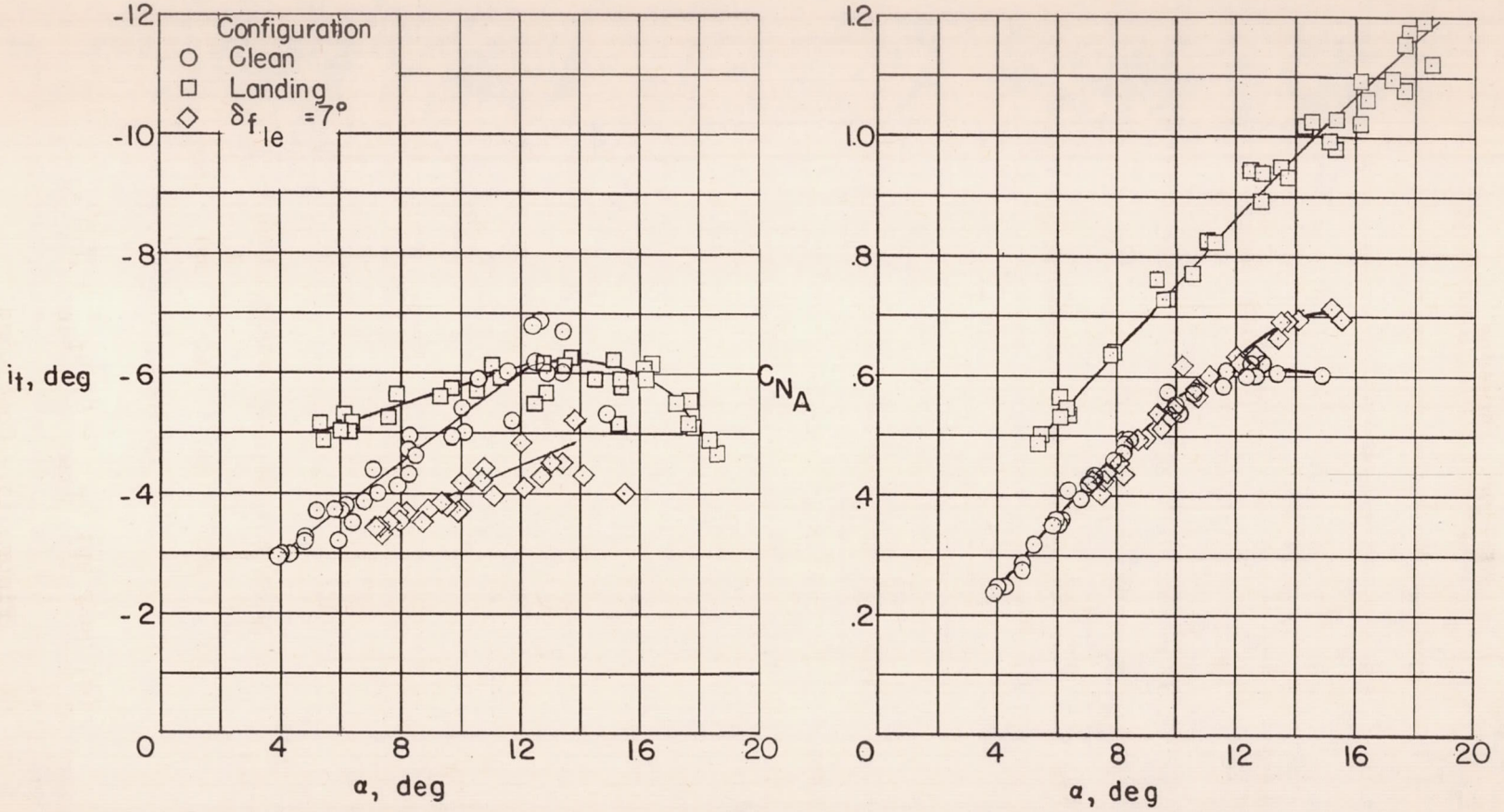

Figure 14.- Variation of i_t and C_{N_A} with α during stall approaches. $h_p \approx 26{,}000$ feet; center of gravity from 3 to -2 percent mean aerodynamic chord. Douglas X-3 research airplane.

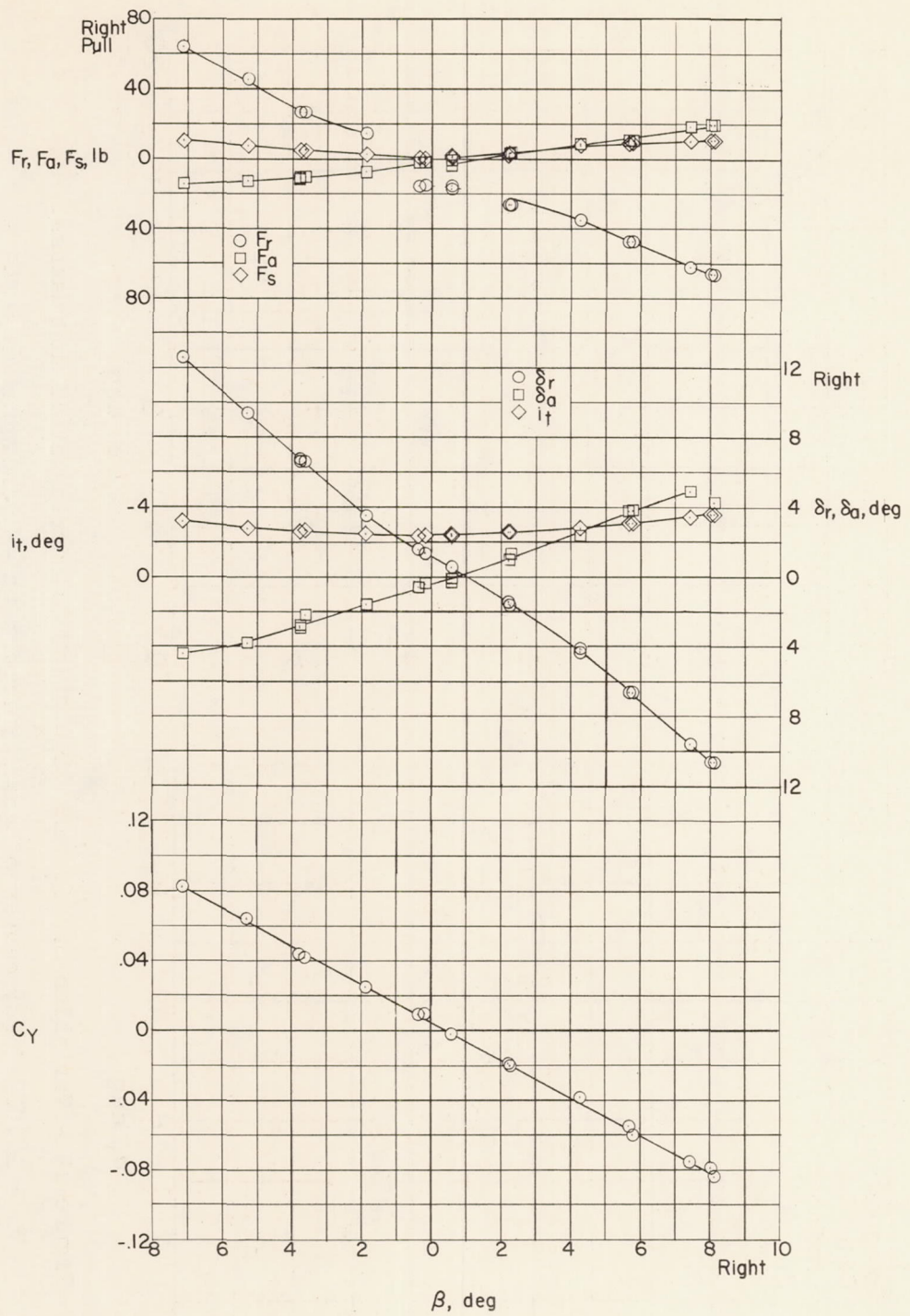

(a) $M \approx 0.84$; $h_p \approx 20{,}000$ feet.

Figure 15.- Variation of control forces, control deflections, and side-force coefficient with sideslip angle during wing-level sideslips. Center of gravity from 3 to -2 percent mean aerodynamic chord. Douglas X-3 research airplane.

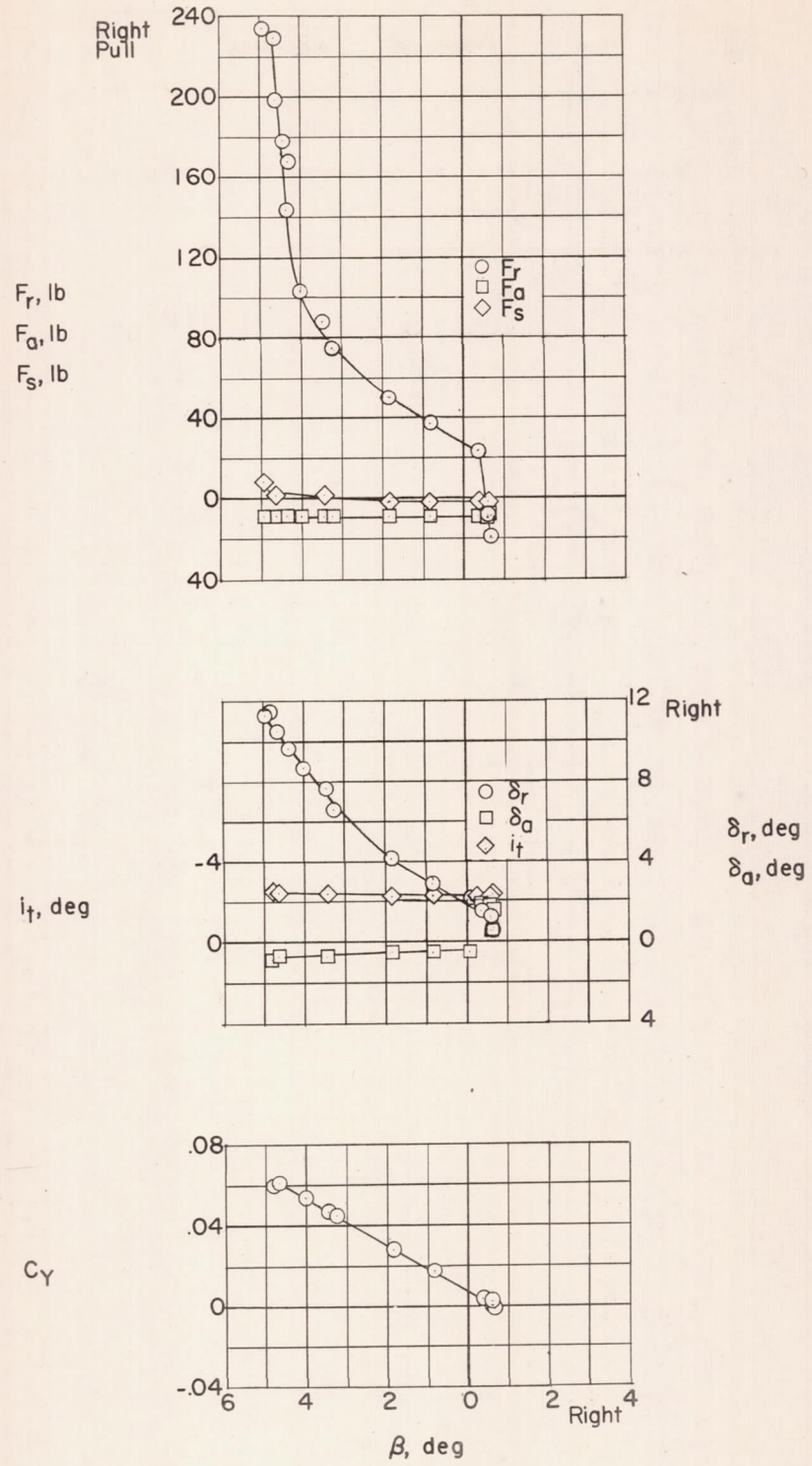

(b) $M \approx 0.96$; $h_p \approx 21{,}000$ feet.

Figure 15.- Continued.

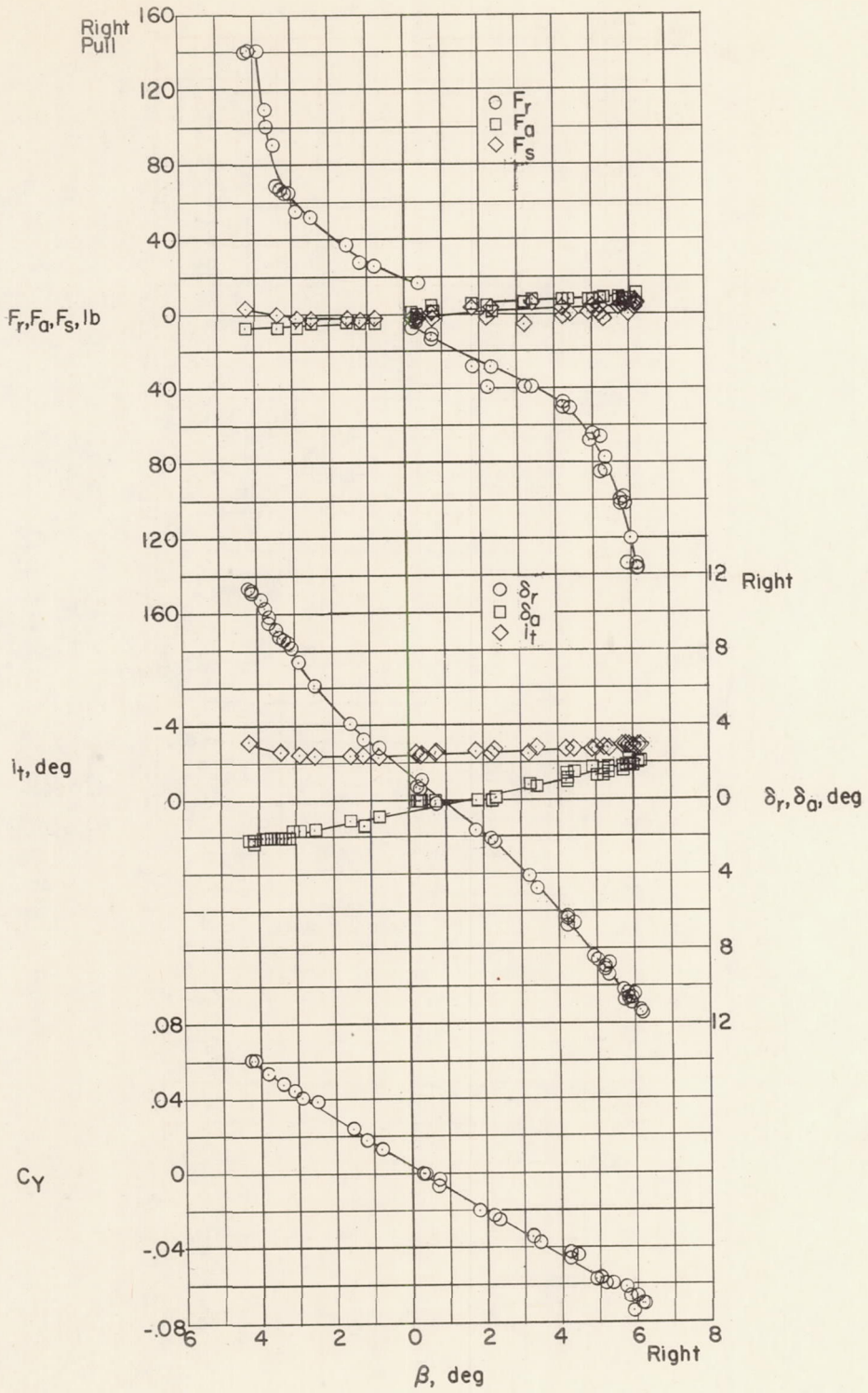

(c) $M \approx 0.98$; $h_p \approx 19{,}800$ feet.

Figure 15.- Concluded.

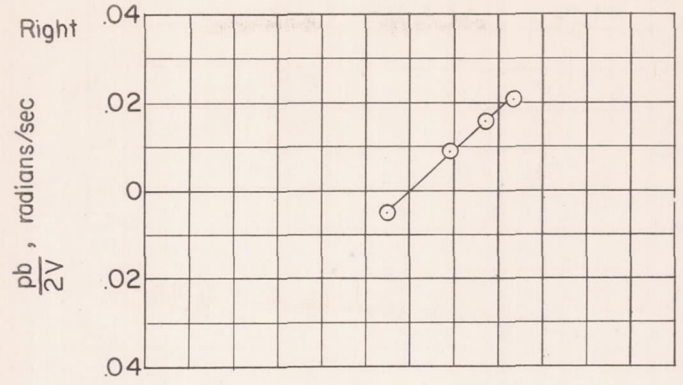

(a) $M \approx 0.89$; $h_p \approx 17{,}000$ feet.

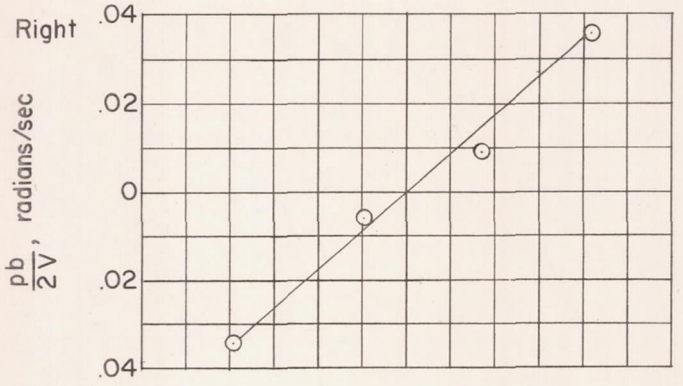

(b) $M \approx 0.94$; $h_p \approx 25{,}000$ feet.

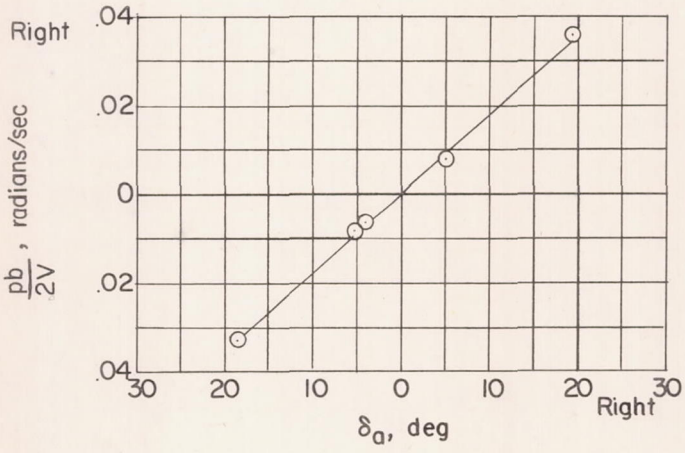

(c) $M \approx 0.98$; $h_p \approx 21{,}000$ feet.

Figure 16.- Variation of wing-tip helix angle with total aileron deflection. Douglas X-3 research airplane.

NACA - Langley Field, Va.